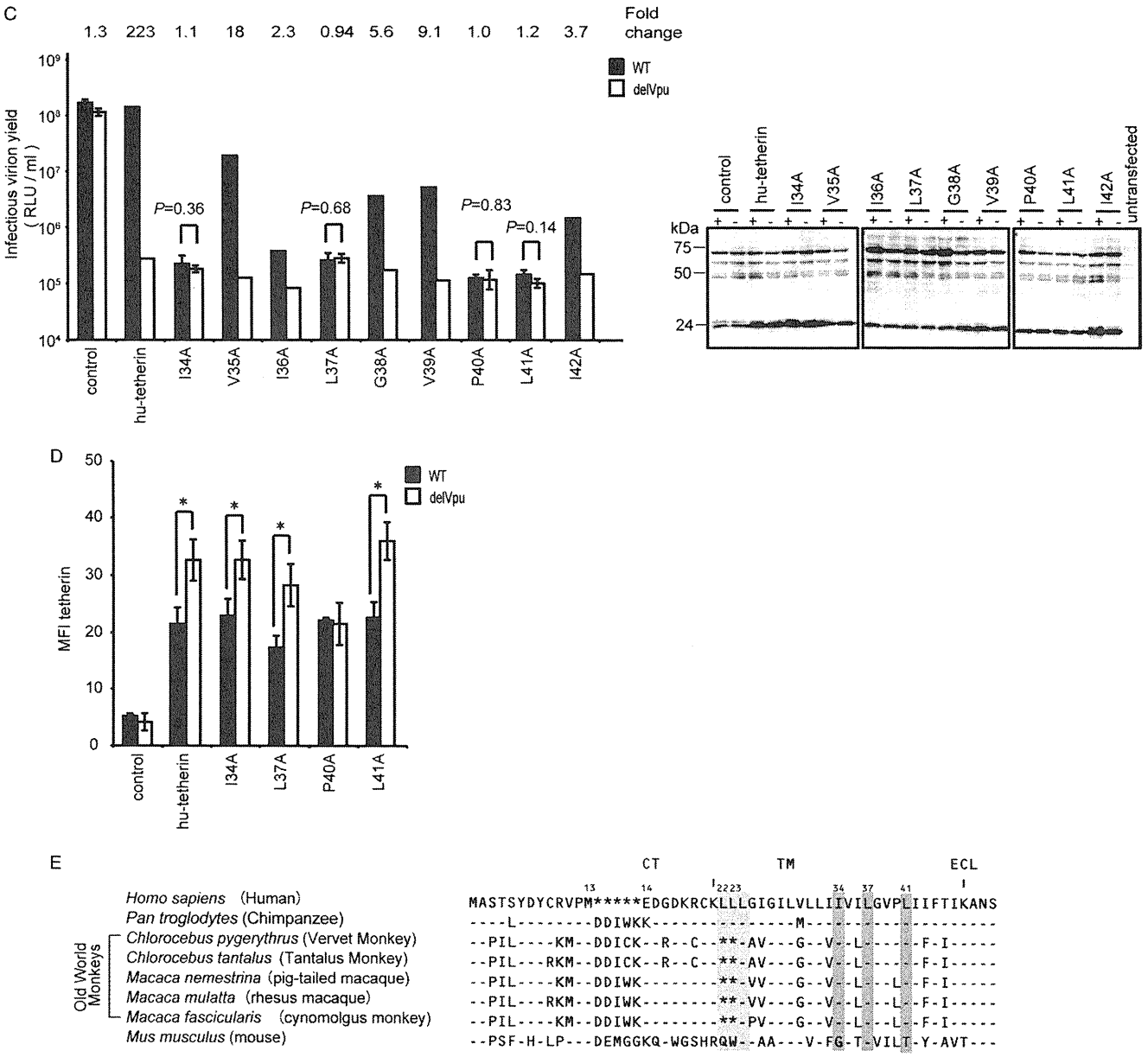

FIG. 3—*Continued.*

mutation of I45T (corresponding to hu-tetherin residues) (Fig. 4A). As demonstrated in Fig. 4C, agm-LL displayed a more-than 2-fold increase of BiFC signal compared to that of WT agm-tetherin. We also tested these mutants for tetherin activity and Vpu sensitivity. Notably, an agm-LL mutant was insensitive to HIV-1 Vpu antagonism (Fig. 4D) even though it interacted with Vpu to a certain extent (Fig. 4C). Finally, the agm-LL/I45T mutant, containing the combined two-leucine insertion and I45T in the TM of agm-tetherin, clearly displayed the Vpu sensitivity (Fig. 4D). However, its BiFC signal was not increased by I45T substitution (Fig. 4C). These results suggest that T45 of hu-tetherin has an important role for Vpu counteraction against tetherin without affecting Vpu-tetherin association.

Structural study of the TM domain of hu- and agm-tetherins in a lipid bilayer environment. To obtain structural insights into the mechanisms by which the amino acid at specific positions in the tetherin TM domain control interaction and susceptibilities to neutralization by Vpu, we constructed 3D models of the TM domains of hu-tetherin, agm-tetherin, and five tetherin mutants, including agm-LL, agm-LL/I45T, hu-delGI, hu-T45I, and hu-delGI/T45I. We constructed these models in a lipid bilayer environment by MD simulations (28, 29, 61) of the models and compared the structures. Representative structures were obtained by cluster analysis (60) of the 3,000 snapshots during 2.0 to 5.0 ns of each MD simulation for the structural comparisons. Details of the simulation methods and processes, such as the time course of structural changes

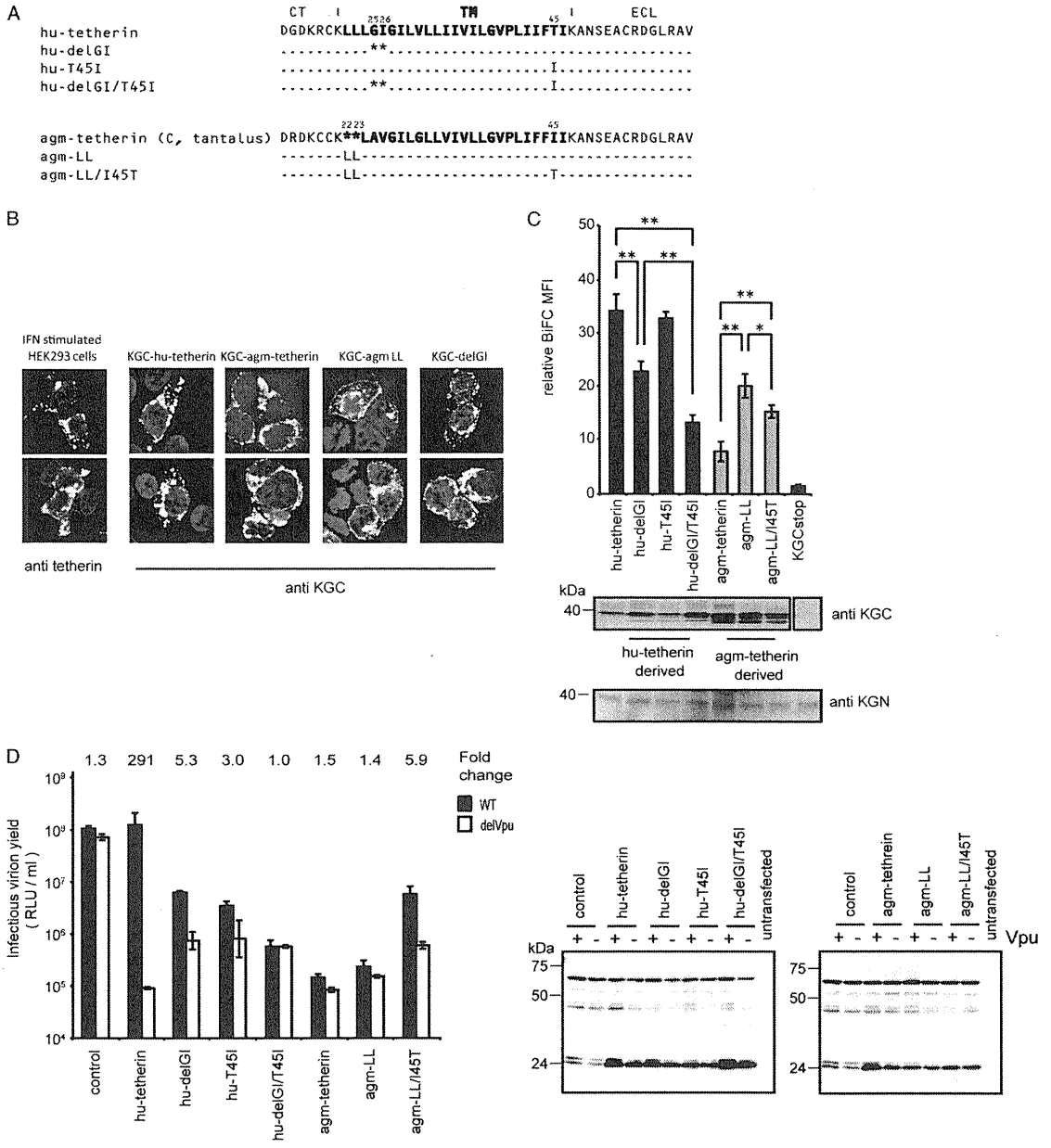

FIG. 4. C-terminal motif in tetherin TM domain is a determinant for Vpu counteraction. (A) Amino acid alignment of hu-tetherin, agm-tetherin, and their mutants. Identity is indicated by dashes, and sequence gaps are indicated by an asterisk. (B) Subcellular localization of tetherin 2-amino acid-deletion mutant or insertion mutant. KGN-Vpu-expressing cells were transfected with plasmid encoding KGC-tagged hu-tetherin, KGC-tagged agm-tetherin, or their mutants, respectively, and cells were stained with an anti-KGC antibody. IFN-treated HEK 293 cells were stained with an anti-tetherin antibody. Cells were examined by confocal microscopy. (C) BiFC assay of hu- and agm-tetherin TM mutants on Vpu interaction. KGN-Vpu-expressing cells were transfected with plasmid encoding KGC-hu-tetherin, KGC-agm-tetherin, or the mutants and was analyzed by flow cytometry. The expression of the protein in cell lysates was detected using the indicated antibody. Relative MFI values are defined as the MFI of pKGC-tetherin or its mutant transfected cells minus the MFI of untransfected cells, and results represent the means from three independent experiments plus standard deviations. (D) Tetherin activity and Vpu sensitivity assays of hu- and agm-tetherin TM mutants. HEK 293 cells were cotransfected as described in the legend to Fig. 2B without (control) or with 100 ng KGC-hu-tetherin or agm-tetherin and the derivative DNA. The HIV-1 proteins ($Pr55^{Gag}$) in the cell lysates were detected using anti-p24 antibody. Results represent the means from three independent experiments plus standard deviations.

during MD simulations, are described in the supplemental material (see Table S1 and Fig. S1 and S2).

The thermodynamically stable hu-tetherin TM model shows that the TM consists of helical structures in the lipid bilayer that are consistent with its location in the plasma membrane. In the model, amino acid residues I34, L37, and L41, which we demonstrated above to be indispensable for Vpu interaction, are positioned on the same face of the helix in the lipid bilayer environment, leading to the protrusion of the hydrophobic side chains in a similar direction (Fig. 5A, amino acid residues with

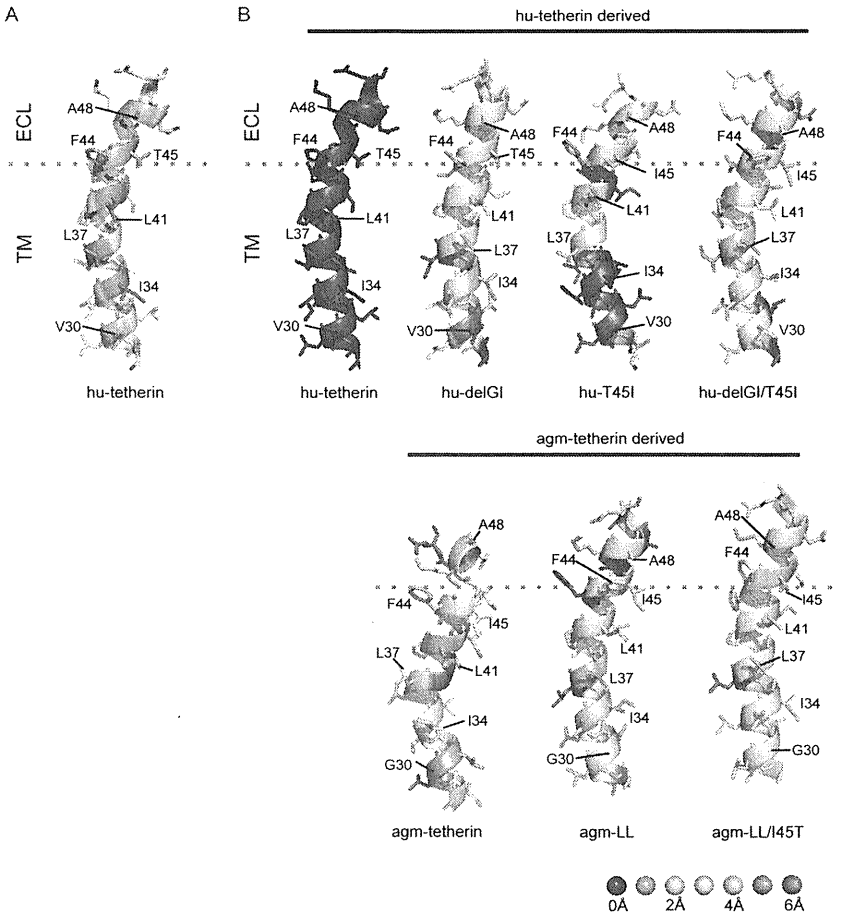

FIG. 5. Structure model of tetherin TM domains. (A) Structural models of C-terminal TM domains (G27 to E51 in hu-tetherin). I34, L37, and L41, whose mutations influence interactions with Vpu, are highlighted with a red cartoon and sticks. V30, F44, T45, and A48, whose side chains are positioned in the same face with side chains of I34, L37, and L41, are highlighted with an orange cartoon and sticks. (B) Comparisons of three-dimensional structures of individual residues between hu-tetherin and others. RMSD values between hu-tetherin and other models were calculated using the coordinates of N, Cα, and C atoms in the C-terminal TM domain (G27 to E51 in hu-tetherin) in the representative structures, each of which was selected from 3,000 snapshots during 2.0 to 5.0 ns of the respective MD simulations using the Bayesian clustering algorithm. The individual residues in the structures were colored according to the RMSD values. The three-dimensional images of the structures were made with PyMOL version 0.99 rc6 (Schrödinger LLC).

red color). V30, F44, T45, and A48 of hu-tetherin also were positioned on the same helical face with these amino acid residues (Fig. 5A, amino acid residues with orange color). This 3D arrangement of particular amino acids on the helical surface was significantly disordered in the TM domains of agm-tetherin; side chains of I34, L37, and L41, which correspond to the I34, L37, and L41 in hu-tetherin, respectively, protruded in different directions (Fig. 5B, agm-tetherin). When the agm-tetherin TM model was superimposed on the hu-tetherin TM model using the main-chain atoms (see Materials and Methods), more than 2.0 Å of 3D positional shifts were detected at the many main-chain atoms. This included I34, L37, F44, I45, and A48, which correspond to I34, L37, F44, T45, and A48, respectively, in hu-tetherin (Fig. 5B; also see Fig. S2 in the supplemental material). On the other hand, conformational changes from the hu-tetherin TM were detected in the smaller regions of other TM variants examined (Fig. 5B, agm-LL, agm-LL/I45T, hu-delGI, hu-T45I, and hu-delGI/T45I). More than 2.0 Å of positional shifts were observed only at I45 of agm-LL, I34 of agm-LL/I45T, A48 of hu-T45I, and F44 and I45 of hu-delGI/T45I (Fig. 5B; also see Fig. S2). hu-delGI was more similar in structure to hu-tetherin than the others (Fig. 5B; also see Fig. S2).

Experimental data showed that I34, L37, and L41 in hu-tetherin are critical for Vpu interaction (Fig. 3B). Hence, we examined how the 3D positions of these amino acid residues are maintained. For hu-T45I, hu-delGI, and agm-LL, which have relatively high competence for Vpu interaction, positional shifts of three amino acid residues were less than 1.3 Å (Fig. 5B; also see Fig. S2). In contrast, the others showed greater positional shifts of the three amino acid residues. Positions of I34 in agm-thetherin and agm-LL/I45T shifted 1.9 to 2.4 Å, while that of L41 in hu-delGI/T45I shifted 1.6 Å. These results are consistent with their competence for Vpu interaction.

Experimental data also pointed out the crucial importance of the amino acid residue at position 45 for the susceptibility of hu-tetherin to Vpu (Fig. 4D). The hu-tetherin and two mutants (agm-LL/I45T and hu-delGI) have threonine at this position and shared relatively similar conformations at the threonine and neighboring phenylalanine (F44 in hu-tetherin); less than

1.5 Å of positional shifts was detected when these mutant TMs were superimposed on the hu-tetherin TM (Fig. 5B; also see Fig. S2). The conformational differences from the hu-tetherin TM were greater for those having the change of threonine into isoleucine (agm-tetherin, agm-LL, hu-T45I, and hu-delGI/T45I); the differences ranged from 1.7 to 3.5 Å with these mutants (Fig. 5B; also see Fig. S2).

We also analyzed the snapshot models at 5.0 ns of each MD simulation. All of these structural characteristics and differences found with the representative models were reproducible with the snapshot model at 5.0 ns of each MD simulation (see Fig. S3 in the supplemental material) where fluctuations of TM structures during MD simulations were relatively small (see Fig. S1). Our structural models support the results that the Vpu-specific interaction and susceptibility with hu-tetherin is defined by critical amino acid residues that lie in the TM (I34, L37, L41, and T45) and imply that the appropriate positioning of these amino acid residues in hu-tetherin are important for Vpu interaction and sensitivity.

DISCUSSION

The molecular basis behind the HIV-1 Vpu counteraction of hu-tetherin has not been fully elucidated. Despite the observation that the specific antagonism of hu-tetherin occurs through a Vpu-mediated pathway, the specific residues of hu-tetherin that define the association with Vpu remain unknown. In this report, we utilized a BiFC approach to characterize the interaction between Vpu and tetherin (Fig. 1). We first validated our BiFC approach by detecting the specific hu-tetherin-Vpu heterodimer complexes (Fig. 1B and D), which have been shown previously by immunoprecipitation studies (25, 54). The complementation-based method is a simple way for confirming the protein-protein interaction in live cells. As BiFC depends on the two interacting proteins to bring the complementary fluorescence protein fragments close enough to fold into stable fluorescence complex, a positive BiFC signal implies a distance of less than 15 nm between the two interacting proteins (33). Consistently with our BiFC results, hu-tetherin and Vpu interaction recently were reported using a fluorescence resonance energy transfer (FRET) assay (2), suggesting a distance of less than 6 nm between the interacting Vpu and tetherin (52). However, it should be noted that although the BiFC assay demonstrated a positive association of tetherin and Vpu, it remains unclear whether the interaction is direct or indirect. As a result, we were able to identify three amino acid residues (I34, L37, and L41) that were shown in our 3D model to align on the same TM helical surface for Vpu interaction (Fig. 5). Altering any one of these amino acid residues led to a disruption of the Vpu-hu-tetherin complex and also abrogated Vpu susceptibility (Fig. 3). Furthermore, our finding that the T45 residue of hu-tetherin had no bearing on the Vpu interaction yet significantly abated Vpu susceptibility (Fig. 4) implies that certain residues participate exclusively in the Vpu-mediated antagonism of tetherin independently of the interaction. In addition, our 3D models offer a glimpse into the possible dynamics of the viral and host molecules and allow us to visualize the arrangement of the amino acid residues in the hu-tetherin TM involved in the possible binding with Vpu.

Recently, several groups have demonstrated that the hu-tetherin TM and specific residues within it are essential for Vpu interaction and hu-tetherin counteraction (10). The studies identified hu-tetherin delGI T45I, delGI I33V I36L (43), del22/23 (54), T45I, and I26V/V30G/I36L/T45I (18) as mutants that are resistant to Vpu, but they mainly focused on hu-tetherin residues that differed from rhesus or agm-tetherin residues (10). In contrast, we conducted a comprehensive screening of the entire TM region and identified three residues (I34, L37, and L41) as critical determinants for Vpu interaction and susceptibility (Fig. 3B and C). Our model predicts that these three amino acid residues are directly involved in helix-helix interactions between the TMs of tetherin and Vpu, composing an interacting domain (Fig. 5A). This possibility is feasible considering the biochemical characteristics of hydrophobic isoleucine and leucine, which often are located at the surfaces of protein-protein interaction sites in membrane proteins, as exemplified in leucine zipper and leucine/isoleucine zipper motifs. The deletion mutants delGI and L22-23 had a significant impact on perturbing the Vpu-mediated antagonism of hu-tetherin (Fig. 4D). Our gain-of-function studies showed that the insertion of two residues (LL) in the TM of agm-tetherin was enough to restore a partial level of interaction with Vpu, and in combination with the I45T mutation, it led to a partial restoration of Vpu sensitivity (Fig. 4D). We speculate that missing residues in the helix, such as the delGI mutant and agm-tetherin, have an overall impact on the TM amino acid residue positioning, thereby affecting both interaction and sensitivity. Interestingly, mutations of L22 and L23 to alanine in our triple-alanine scan mutants disrupted Vpu interaction, whereas mutations of G25 and I26 to alanine did not have any effect (Fig. 3A). This finding leads us to believe that the deletion of LL has a more-specific effect on the Vpu interaction in conjunction with orienting the tetherin helix TM residues.

In an evolutionary aspect, two amino acids in the hu-tetherin TM might have been inserted when advanced primates evolved from primitive primates, resulting in an adaptation by HIV-1 Vpu to recognize hu-tetherin. It is unclear why these insertions at positions 22 and 23 occur in hu-tetherin, but the fact that these regions also evolved under selective pressure shows that these events might have occurred as a consequence of their role in other functional activities of tetherin, such as B cell differentiation, the inhibition of virus production, or the regulation of interferon release (6, 18, 24, 43).

In contrast to other reports (10), we could not definitively verify the importance of the mutant I36A. The mutation of I36 did not have an impact on the Vpu and hu-tetherin interaction in our BiFC assay; even though it attenuated Vpu susceptibility during virus release, the effect was not as dramatic as mutating L34, L37, L41, or T45 (Fig. 3B and C and 4C and D). Mutants I26A and V30A were not investigated further, because they did not disrupt the Vpu and tetherin BiFC fluorophore in our preliminary interaction screen (Fig. 3A).

Interestingly, a P40A mutation also abolished susceptibility to Vpu (Fig. 3C), although McNatt et al. reported that a P40I mutation does not affect the Vpu susceptibility (43). However, this discrepancy more likely is due to an overall conformational rearrangement of the hu-tetherin TM from the replacement of proline with hydrophobic amino acid of different sizes. Proline residues generally play significant roles in maintaining the conformational structure, and

changing proline to alanine can affect the overall conformation more dramatically than changing proline to isoleucine (53). In addition to P40A, I36A also displayed, to a lesser extent, Vpu counteraction (Fig. 3C). In a previous study, I36 has been shown to be one of the positively selected residues in the hu-tetherin TM sequence (18, 43). When this residue was exchanged for alanine, a loss of susceptibility to Vpu was observed (Fig. 3C). From our structural analysis of human tetherin, I36 is not likely to be involved in interaction; however, exchanging I36 for other residues can affect Vpu susceptibility.

One of the more-important observations of our study was the function of T45, which repeatedly has been reported to be essential for Vpu susceptibility by others (10, 18, 43). In our hands, a mutation of this residue did not significantly affect Vpu and hu-tetherin complex formation when measuring the interaction by BiFC; however, the mutation of T45 still affected Vpu sensitivity (Fig. 4D). Our gain-of-function studies further illustrated the importance of T45 by rendering agm-tetherin susceptible to Vpu in the agm-LL/I45T mutant, an effect that was not observed for the agm-LL mutant without the I45T substitution. This suggests that Vpu-tetherin association alone is not sufficient for acquiring antagonistic activity.

Changes in the amino acid at position 45 in hu-tetherin TM are predicted to influence the conformation of not only itself but also its immediate downstream amino acid at position 44 (Fig. 5B; also see Fig. S2 in the supplemental material). When hu-tetherin has a threonine at position 45, the amino acids at positions 44 and 45 tended to be positioned on the same surface as the functionally important amino acid, such as I34, L37, and L41 (Fig. 4B; also see Fig. S4). Concurrently with this folding property, tetherins tended to preserve the Vpu-susceptibility (Fig. 4D, hu-delGI). In contrast, when agm-tetherin has an isoleucine at position 45, the ordered 3D arrangement fluctuated, particularly at positions 44 and 45, and the tetherins tended to have severely reduced susceptibilities to Vpu activity (Fig. 4D and 5B; also see Table S1 and Fig. S2). These results indicate that the amino acid at position 45 plays crucial roles in both folding and the Vpu susceptibility of the hu-tetherin TM domain. This is consistent with biochemical characteristics of threonine; in general, threonine is rare in TMs of proteins; however, if it exists, the threonine can play very important roles in the folding and protein-protein interaction of TMs (49), such as the tight packing of helices (14), the formation of intermolecular hydrogen bonds (13, 62), and the formation of biologically functional protein complexes (3). Therefore, it is conceivable that T45 in hu-tetherin plays key roles in forming a biologically functional complex of hu-tetherin, Vpu, and undefined proteins for the Vpu-mediated degradation of tetherin. T45 may play an important role in one or more of the reported mechanisms by which Vpu antagonizes hu-tetherin: (i) by targeting hu-tetherin for proteasomal and/or lysosomal degradation via the β-TrCP-dependent ubiquitin/proteasome pathway (10); (ii) by trafficking hu-tetherin to intracellular organelles such as the TGN, Golgi complex, or ER (12); and (iii) by sequestering hu-tetherin within intracellular compartments and preventing its distribution to the plasma membrane (11, 19). Although our results indicate that T45 behaves in this manner, residues identified by Gupta et al., such as I26, V30, and I36, also may contribute similarly (18). Further structural and biochemical studies are necessary to address this issue.

In conclusion, the main advantage our modeling results provides is the visualization and positioning of the TM amino acid residues in a manner that allows for Vpu binding. To our knowledge, this is the first 3D model for the TM domain of tetherin that offers a plausible explanation for the residues involved in the Vpu-hu-tetherin interaction. Having this insight will aid in identifying the complementary motifs in Vpu that interact with the three amino acid residues found in this study. Our BiFC system also will be a useful tool for building a structure-activity relationship and elucidating the Vpu TM residues contributing to tetherin binding. Moreover, it also is conceivable to design a type of peptide decoy molecule (45) consisting of only a TM domain homologous to human tetherin that is able to sequester Vpu while permitting the retainment of HIV-1 virions by tetherin. With this in mind, and guided by structure-based predictions, the Vpu-tetherin complex could become a novel target for the future pharmacological intervention of HIV-1 dissemination.

ACKNOWLEDGMENTS

We thank Jun Komano and Chuanyi Nie for helpful discussions of the manuscript.

This work was supported by Grants-in-Aid for Science Research of Priority Areas from the Ministry of Education, Culture, Sports and Technology of Japan, a Health and Labor Science research grant (Research on Publicly Essential Drugs and Medical Devices) and a grant for HIV/AIDS research from the Ministry of Health, Labor and Welfare of Japan. K.S., T.Y., and S.P.Y. were supported by research fellowships from the Japan Society for the Promotion of Science for Young Scientists.

REFERENCES

1. **Andrew, A. J., E. Miyagi, S. Kao, and K. Strebel.** 2009. The formation of cysteine-linked dimers of BST-2/tetherin is important for inhibition of HIV-1 virus release but not for sensitivity to Vpu. Retrovirology **6**:80.
2. **Banning, C., J. Votteler, D. Hoffmann, H. Koppensteiner, M. Warmer, R. Reimer, F. Kirchhoff, U. Schubert, J. Hauber, and M. Schindler.** 2010. A flow cytometry-based FRET assay to identify and analyse protein-protein interactions in living cells. PLoS One **5**:e9344.
3. **Beahm, D. L., A. Oshima, G. M. Gaietta, G. M. Hand, A. E. Smock, S. N. Zucker, M. M. Toloue, A. Chandrasekhar, B. J. Nicholson, and G. E. Sosinsky.** 2006. Mutation of a conserved threonine in the third transmembrane helix of alpha- and beta-connexins creates a dominant-negative closed gap junction channel. J. Biol. Chem. **281**:7994–8009.
4. **Bieniasz, P. D.** 2009. The cell biology of HIV-1 virion genesis. Cell Host Microbe **5**:550–558.
5. **Brügger, B., B. Glass, P. Haberkant, I. Leibrecht, F. T. Wieland, and H. G. Krausslich.** 2006. The HIV lipidome: a raft with an unusual composition. Proc. Natl. Acad. Sci. U. S. A. **103**:2641–2646.
6. **Cao, W., L. Bover, M. Cho, X. Wen, S. Hanabuchi, M. Bao, D. B. Rosen, Y. H. Wang, J. L. Shaw, Q. Du, C. Li, N. Arai, Z. Yao, L. L. Lanier, and Y. J. Liu.** 2009. Regulation of TLR7/9 responses in plasmacytoid dendritic cells by BST2 and ILT7 receptor interaction. J. Exp. Med. **206**:1603–1614.
7. **Cohen, E. A., E. F. Terwilliger, J. G. Sodroski, and W. A. Haseltine.** 1988. Identification of a protein encoded by the vpu gene of HIV-1. Nature **334**:532–534.
8. **Crowley, M. F., T. A. Darden, T. E. Cheatham, and D. W. Deerfield.** 1997. Adventures in improving the scaling and accuracy of a parallel molecular dynamics program. J. Supercomput. **11**:255–278.
9. **Darden, T., D. York, and L. Pedersen.** 1993. Particle mesh Ewald–an Nlog(N) method for Ewald sums in large systems. J. Chem. Phys. **98**:10089–10092.
10. **Douglas, J. L., J. K. Gustin, K. Viswanathan, M. Mansouri, A. V. Moses, and K. Fruh.** 2010. The great escape: viral strategies to counter BST-2/tetherin. PLoS Pathog. **6**:e1000913.

11. **Dubé, M., B. B. Roy, P. Guiot-Guillain, J. Binette, J. Mercier, A. Chiasson, and E. A. Cohen.** 2010. Antagonism of tetherin restriction of HIV-1 release by Vpu involves binding and sequestration of the restriction factor in a perinuclear compartment. PLoS Pathog. **6**:e1000856.
12. **Dubé, M., B. B. Roy, P. Guiot-Guillain, J. Mercier, J. Binette, G. Leung, and E. A. Cohen.** 2009. Suppression of tetherin-restricting activity upon human immunodeficiency virus type 1 particle release correlates with localization of Vpu in the trans-Golgi network. J. Virol. **83**:4574–4590.
13. **Duong, M. T., T. M. Jaszewski, K. G. Fleming, and K. R. MacKenzie.** 2007. Changes in apparent free energy of helix-helix dimerization in a biological membrane due to point mutations. J. Mol. Biol. **371**:422–434.
14. **Eilers, M., S. C. Shekar, T. Shieh, S. O. Smith, and P. J. Fleming.** 2000. Internal packing of helical membrane proteins. Proc. Natl. Acad. Sci. U. S. A. **97**:5796–5801.
15. **Essmann, U., L. Perera, M. L. Berkowitz, T. Darden, H. Lee, and L. G. Pedersen.** 1995. A smooth particle mesh Ewald method. J. Chem. Phys. **103**:8577–8593.
16. **Fritsch, V., G. Ravishanker, D. L. Beveridge, and E. Westhof.** 1993. Molecular dynamics simulations of poly(dA) · poly(dT): comparisons between implicit and explicit solvent representations. Biopolymers **33**:1537–1552.
17. **Goffinet, C., I. Allespach, S. Homann, H. M. Tervo, A. Habermann, D. Rupp, L. Oberbremer, C. Kern, N. Tibroni, S. Welsch, J. Krijnse-Locker, G. Banting, H. G. Krausslich, O. T. Fackler, and O. T. Keppler.** 2009. HIV-1 antagonism of CD317 is species specific and involves Vpu-mediated proteasomal degradation of the restriction factor. Cell Host Microbe **5**:285–297.
18. **Gupta, R. K., S. Hue, T. Schaller, E. Verschoor, D. Pillay, and G. J. Towers.** 2009. Mutation of a single residue renders human tetherin resistant to HIV-1 Vpu-mediated depletion. PLoS Pathog. **5**:e1000443.
19. **Hauser, H., L. A. Lopez, S. J. Yang, J. E. Oldenburg, C. M. Exline, J. C. Guatelli, and P. M. Cannon.** 2010. HIV-1 Vpu and HIV-2 Env counteract BST-2/tetherin by sequestration in a perinuclear compartment. Retrovirology **7**:51.
20. **Hornak, V., R. Abel, A. Okur, B. Strockbine, A. Roitberg, and C. Simmerling.** 2006. Comparison of multiple Amber force fields and development of improved protein backbone parameters. Proteins **65**:712–725.
21. **Hout, D. R., E. R. Mulcahy, E. Pacyniak, L. M. Gomez, M. L. Gomez, and E. B. Stephens.** 2004. Vpu: a multifunctional protein that enhances the pathogenesis of human immunodeficiency virus type 1. Curr. HIV Res. **2**:255–270.
22. **Humphrey, W., A. Dalke, and K. Schulten.** 1996. VMD: visual molecular dynamics. J. Mol. Graph. **14**:27–38.
23. **Ibragimova, G. T., and R. C. Wade.** 1998. Importance of explicit salt ions for protein stability in molecular dynamics simulation. Biophys. J. **74**:2906–2911.
24. **Ishikawa, J., T. Kaisho, H. Tomizawa, B. O. Lee, Y. Kobune, J. Inazawa, K. Oritani, M. Itoh, T. Ochi, K. Ishihara, et al.** 1995. Molecular cloning and chromosomal mapping of a bone marrow stromal cell surface gene, BST2, that may be involved in pre-B-cell growth. Genomics **26**:527–534.
25. **Iwabu, Y., H. Fujita, M. Kinomoto, K. Kaneko, Y. Ishizaka, Y. Tanaka, T. Sata, and K. Tokunaga.** 2009. HIV-1 accessory protein Vpu internalizes cell-surface BST-2/tetherin through transmembrane interactions leading to lysosomes. J. Biol. Chem. **284**:35060–35072.
26. **Jójárt, B., and T. A. Martinek.** 2007. Performance of the general amber force field in modeling aqueous POPC membrane bilayers. J. Comput. Chem. **28**:2051–2058.
27. **Jorgensen, W. L., J. Chandrasekhar, J. Madura, and M. L. Klein.** 1983. Comparison of simple potential functions for simulating liquid water. J. Chem. Phys. **79**:926–935.
28. **Kandasamy, S. K., and R. G. Larson.** 2006. Molecular dynamics simulations of model trans-membrane peptides in lipid bilayers: a systematic investigation of hydrophobic mismatch. Biophys. J. **90**:2326–2343.
29. **Karplus, M., and J. A. McCammon.** 2002. Molecular dynamics simulations of biomolecules. Nat. Struct. Biol. **9**:646–652.
30. **Kawano, Y., T. Yoshida, K. Hieda, J. Aoki, H. Miyoshi, and Y. Koyanagi.** 2004. A lentiviral cDNA library employing lambda recombination used to clone an inhibitor of human immunodeficiency virus type 1-induced cell death. J. Virol. **78**:11352–11359.
31. **Kerppola, T. K.** 2006. Complementary methods for studies of protein interactions in living cells. Nat. Methods **3**:969–971.
32. **Kerppola, T. K.** 2006. Design and implementation of bimolecular fluorescence complementation (BiFC) assays for the visualization of protein interactions in living cells. Nat. Protoc. **1**:1278–1286.
33. **Kerppola, T. K.** 2006. Visualization of molecular interactions by fluorescence complementation. Nat. Rev. Mol. Cell Biol. **7**:449–456.
34. **Klimkait, T., K. Strebel, M. D. Hoggan, M. A. Martin, and J. M. Orenstein.** 1990. The human immunodeficiency virus type 1-specific protein vpu is required for efficient virus maturation and release. J. Virol. **64**:621–629.
35. **Kollman, P. A., I. Massova, C. Reyes, B. Kuhn, S. Huo, L. Chong, M. Lee, T. Lee, Y. Duan, W. Wang, O. Donini, P. Cieplak, J. Srinivasan, D. A. Case, and T. E. I. Cheatham.** 2000. Calculating structures and free energies of complex molecules: combining molecular mechanics and continuum models. Acc. Chem. Res. **33**:889–897.
36. **Kupzig, S., V. Korolchuk, R. Rollason, A. Sugden, A. Wilde, and G. Banting.** 2003. Bst-2/HM1.24 is a raft-associated apical membrane protein with an unusual topology. Traffic **4**:694–709.
37. **Lefèvre, F., M. H. Remy, and J. M. Masson.** 1997. Alanine-stretch scanning mutagenesis: a simple and efficient method to probe protein structure and function. Nucleic Acids Res. **25**:447–448.
38. **Lim, E. S., H. S. Malik, and M. Emerman.** 2010. Ancient adaptive evolution of tetherin shaped the functions of Vpu and Nef in human immunodeficiency virus and primate lentiviruses. J. Virol. **84**:7124–7134.
39. **Loncharich, R. J., B. R. Brooks, and R. W. Pastor.** 1992. Langevin dynamics of peptides: the frictional dependence of isomerization rates of N-actylanayl-N′-methylamide. Biopolymers **32**:523–535.
40. **Maldarelli, F., M. Y. Chen, R. L. Willey, and K. Strebel.** 1993. Human immunodeficiency virus type 1 Vpu protein is an oligomeric type I integral membrane protein. J. Virol. **67**:5056–5061.
41. **Mangeat, B., G. Gers-Huber, M. Lehmann, M. Zufferey, J. Luban, and V. Piguet.** 2009. HIV-1 Vpu neutralizes the antiviral factor tetherin/BST-2 by binding it and directing its beta-TrCP2-dependent degradation. PLoS Pathog. **5**:e1000574.
42. **Masuyama, N., T. Kuronita, R. Tanaka, T. Muto, Y. Hirota, A. Takigawa, H. Fujita, Y. Aso, J. Amano, and Y. Tanaka.** 2009. HM1.24 is internalized from lipid rafts by clathrin-mediated endocytosis through interaction with alpha-adaptin. J. Biol. Chem. **284**:15927–15941.
43. **McNatt, M. W., T. Zang, T. Hatziioannou, M. Bartlett, I. B. Fofana, W. E. Johnson, S. J. Neil, and P. D. Bieniasz.** 2009. Species-specific activity of HIV-1 Vpu and positive selection of tetherin transmembrane domain variants. PLoS Pathog. **5**:e1000300.
44. **Miaskiewicz, K., R. Osman, and H. Weinstein.** 1993. Molecular dynamics simulation of the hydrated d(CGCGamino acidTTCGCG)2 dodecamer. J. Am. Chem. Soc. **115**:1526–1537.
45. **Montal, M.** 2009. Vpu matchmakers as a therapeutic strategy for HIV infection. PLoS Pathog. **5**:e1000246.
46. **Neil, S. J., T. Zang, and P. D. Bieniasz.** 2008. Tetherin inhibits retrovirus release and is antagonized by HIV-1 Vpu. Nature **451**:425–430.
47. **Nguyen, K. L., M. llano, H. Akari, E. Miyagi, E. M. Poeschla, K. Strebel, and S. Bour.** 2004. Codon optimization of the HIV-1 vpu and vif genes stabilizes their mRNA and allows for highly efficient Rev-independent expression. Virology **319**:163–175.
48. **Nilsson, L.** 1998. Protein nucleic acid interactions, p. 2220–2229. *In* P. von Ragué Schleyer, et al. (ed.), Encyclopedia of computational chemistry. John Wiley & Sons, New York, NY.
49. **Nyholm, T. K., S. Ozdirekcan, and J. A. Killian.** 2007. How protein transmembrane segments sense the lipid environment. Biochemistry **46**:1457–1465.
50. **Pastor, R. W., B. R. Brooks, and A. Szabo.** 1988. An analysis of the accuracy of Langevin and molecular dynamics algorithms. Mol. Phys. **65**:1409–1419.
51. **Pearlman, D. A., D. A. Case, J. W. Caldwell, W. S. Ross, T. E. I. Cheatham, S. DeBolt, D. Ferguson, G. Seibel, and P. Kollman.** 1995. AMBER, a package of computer programs for applying molecular mechanics, normal mode analysis, molecular dynamics and free energy calculations to simulate the structural and energetic properties of molecules. Comp. Phys. Commun. **91**:1–41.
52. **Poole, E., P. Strappe, H. P. Mok, R. Hicks, and A. M. Lever.** 2005. HIV-1 Gag-RNA interaction occurs at a perinuclear/centrosomal site; analysis by confocal microscopy and FRET. Traffic **6**:741–755.
53. **Ramachandran, G. N., C. Ramakrishnan, and V. Sasisekharan.** 1963. Stereochemistry of polypeptide chain configurations. J. Mol. Biol. **7**:95–99.
54. **Rong, L., J. Zhang, J. Lu, Q. Pan, R. P. Lorgeoux, C. Aloysius, F. Guo, S. L. Liu, M. A. Wainberg, and C. Liang.** 2009. The transmembrane domain of BST-2 determines its sensitivity to down-modulation by human immunodeficiency virus type 1 Vpu. J. Virol. **83**:7536–7546.
55. **Ryckaert, J.-P., G. Ciccotti, and H. J. C. Berendsen.** 1977. Numerical integration of the Cartesian equations of motion of a system with constraints: molecular dynamics of n-alkanes. J. Comput. Phys. **23**:327–341.
56. **Sato, K., S. P. Yamamoto, N. Misawa, T. Yoshida, T. Miyazawa, and Y. Koyanagi.** 2009. Comparative study on the effect of human BST-2/tetherin on HIV-1 release in cells of various species. Retrovirology **6**:53.
57. **Sauter, D., M. Schindler, A. Specht, W. N. Landford, J. Munch, K. A. Kim, J. Votteler, U. Schubert, F. Bibollet-Ruche, B. F. Keele, J. Takehisa, Y. Ogando, C. Ochsenbauer, J. C. Kappes, A. Ayouba, M. Peeters, G. H. Learn, G. Shaw, P. M. Sharp, P. Bieniasz, B. H. Hahn, T. Hatziioannou, and F. Kirchhoff.** 2009. Tetherin-driven adaptation of Vpu and Nef function and the evolution of pandemic and nonpandemic HIV-1 strains. Cell Host Microbe **6**:409–421.
58. **Schubert, U., S. Bour, A. V. Ferrer-Montiel, M. Montal, F. Maldarell, and K. Strebel.** 1996. The two biological activities of human immunodeficiency virus type 1 Vpu protein involve two separable structural domains. J. Virol. **70**: 809–819.
59. **Schubert, U., and K. Strebel.** 1994. Differential activities of the human immunodeficiency virus type 1-encoded Vpu protein are regulated by phosphorylation and occur in different cellular compartments. J. Virol. **68**:2260–2271.
60. **Shao, J., S. W. Tanner, N. Thompson, and T. E. Cheatham.** 2007. Clustering

molecular dynamics trajectories. 1. Characterizing the performance of different clustering algorithms. J. Chem. Theory Comput. **3**:2312–2334.
61. **Shen, L., D. Bassolino, and T. Stouch.** 1997. Transmembrane helix structure, dynamics, and interactions: multi-nanosecond molecular dynamics simulations. Biophys. J. **73**:3–20.
62. **Smith, S. O., M. Eilers, D. Song, E. Crocker, W. Ying, M. Groesbeck, G. Metz, M. Ziliox, and S. Aimoto.** 2002. Implications of threonine hydrogen bonding in the glycophorin A transmembrane helix dimer. Biophys. J. **82**: 2476–2486.
63. **Strebel, K., T. Klimkait, and M. A. Martin.** 1988. A novel gene of HIV-1, vpu, and its 16-kilodalton product. Science **241**:1221–1223.
64. **Strebel, K., J. Luban, and K. T. Jeang.** 2009. Human cellular restriction factors that target HIV-1 replication. BMC Med. **7**:48.
65. **Tokarev, A., M. Skasko, K. Fitzpatrick, and J. Guatelli.** 2009. Antiviral activity of the interferon-induced cellular protein BST-2/tetherin. AIDS Res. Hum. Retrovir. **25**:1197–1210.
66. **Ueyama, T., T. Kusakabe, S. Karasawa, T. Kawasaki, A. Shimizu, J. Son, T. L. Leto, A. Miyawaki, and N. Saito.** 2008. Sequential binding of cytosolic Phox complex to phagosomes through regulated adaptor proteins: evaluation using the novel monomeric Kusabira-Green system and live imaging of phagocytosis. J. Immunol. **181**:629–640.
67. **Van Damme, N., D. Goff, C. Katsura, R. L. Jorgenson, R. Mitchell, M. C. Johnson, E. B. Stephens, and J. Guatelli.** 2008. The interferon-induced protein BST-2 restricts HIV-1 release and is downregulated from the cell surface by the viral Vpu protein. Cell Host Microbe **3**:245–252.
68. **van Meer, G., D. R. Voelker, and G. W. Feigenson.** 2008. Membrane lipids: where they are and how they behave. Nat. Rev. Mol. Cell Biol. **9**:112–124.
69. **Wang, J., R. M. Wolf, J. W. Caldwell, P. A. Kollman, and D. A. Case.** 2004. Development and testing of a general amber force field. J. Comput. Chem. **25**:1157–1174.
70. **Willey, R. L., F. Maldarelli, M. A. Martin, and K. Strebel.** 1992. Human immunodeficiency virus type 1 Vpu protein regulates the formation of intracellular gp160-CD4 complexes. J. Virol. **66**:226–234.
71. **Yoshida, T., H. Ebina, and Y. Koyanagi.** 2009. N-linked glycan-dependent interaction of CD63 with CXCR4 at the Golgi apparatus induces downregulation of CXCR4. Microbiol. Immunol. **53**:629–635.

Published online on 12 July 2011 Exp Biol Med, doi: 10.1258/ebm.2011.010294

Minireview

The mouse is out of the bag: insights and perspectives on HIV-1-infected humanized mouse models

Kei Sato[1] and Yoshio Koyanagi[1,2]

[1]Center for Emerging Virus Research; [2]Laboratory of Viral Pathogenesis, Institute for Virus Research, Kyoto University, 53 Shogoinkawara-cho, Sakyo-ku, Kyoto 606-8507, Japan
Corresponding authors: Kei Sato or Yoshio Koyanagi. Emails: ksato@virus.kyoto-u.ac.jp or ykoyanag@virus.kyoto-u.ac.jp

Abstract

Human immunodeficiency virus type 1 (HIV-1), which is the causative agent of acquired immunodeficiency syndrome, is a human-specific virus. Because HIV-1 cannot infect and cause disorders in other animals, it has been an arduous struggle to study the dynamics of HIV-1 infection *in vivo*. To understand and elucidate HIV-1 pathogenesis *in vivo*, several small animal models for HIV-1 infection have been established and improved over the last 20 years. Recently, a novel murine model, 'humanized mouse', has been generated. A humanized mouse has the potential to maintain human hematopoiesis including human $CD4^+$ leukocytes and, therefore, is able to support persistent HIV-1 infection *in vivo*. We herein describe the current state-of-the-art in HIV-1-infected humanized mice and introduce insights and perspectives of their use for HIV-1 studies *in vivo*.

Keywords: humanized mouse, human hematopoiesis, HIV-1

Experimental Biology and Medicine 2011: 1–9. DOI: 10.1258/ebm.2011.010294

Introduction

Although there are numerous kinds of viruses in the world, some pathogenic viruses such as human immunodeficiency virus type 1 (HIV-1) and Epstein–Barr virus (EBV) are species-specific and can only infect and/or cause disease in humans. Since such human-specific viruses are unable to induce disorders in other animals, it has been almost impossible to investigate the dynamics of virulence and pathogenesis caused by human-specific pathogens in a non-human *in vivo* model.

In particular, to investigate and simulate HIV-1 infection including acquired immunodeficiency syndrome (AIDS) in humans, rhesus macaque monkeys infected with simian immunodeficiency virus (SIV), an evolutionary analogous virus to HIV-1, have been widely utilized and adopted. Nevertheless, it may be presumptuous to assume that SIV pathogenesis in macaques is identical to HIV-1 pathogenesis in humans. Indeed, it has been recently reported that an anti-HIV-1 vaccination trial for high-risk individuals, which was shown to be elegantly successful in an experimental SIV/macaque model, was prematurely terminated due to an increased frequency of seroconversion in the vaccinees.[1–3] This result serves as a caveat implying that we should consider the potential extent of virulence of human-specific viruses including HIV-1 by using multiple experimental models. Furthermore, for an in-depth understanding of the pathogenesis of HIV-1 itself *in vivo*, novel animal models, which support HIV-1 infection, have been generated. In this review, we briefly introduce the history of the ongoing trial for a system capable of supporting HIV-1 infection in mice that has spanned over approximately two decades. Moreover, we go in-depth to describe the cutting-edge investigations of HIV-1 infection in a novel experimental mouse model, called 'humanized mouse'.

The road to 'humanized mice': the history and the usage

In order to evaluate the effectiveness of anti-HIV-1 drugs and vaccines *in vivo*, extensive attempts have been performed to generate cost-effective and ease of use monitoring of HIV-1 pathogenesis in a small animal model. In 1983, Bosma *et al.*[4] established the CB17-*scid* mouse that has a spontaneous autosomal recessive mutation in the *Prkdc* gene causing severe combined immunodeficiency (SCID), called $Prkdc^{scid}$. By using this mouse strain as the recipient, an initial successful trial was reported in 1988: the CB17-*scid* mice were surgically co-implanted with approximately 1-mm pieces of aborted human fetal thymus and liver under the kidney capsule, and the resulting chimeric

ISSN: 1535-3702

Table 1 Comparison of the established human/mouse chimeric models for HIV-1 infection

General designation (established)*	Source†	Reconstitution of human cells		HIV-1 infection	
		Lineage	Duration	Target	Systemic infection (RNA copies/mL plasma)
SCID-hu thy/liv mice (1988)	Fetal thymus and liver	Thymocytes	More than 1 year	CD4SP and DP thymocytes	
Hu-PBL-SCID mice (1991)	Human PBMCs	Xenoreactive T-cells	A few months	Activated CD4 T-cells	10^5–10^7
Humanized mice (2006)	Human HSCs	Lines of human leukocytes	More than 1 year	CD4 T-cells, macrophages, dendritic cells	10^3–10^5

PBMC, peripheral blood mononuclear cell; HSC, hematopoietic stem cell; SP, single positive; DP, CD4CD8 double positive
*The general designation of the established chimeric mice. The A.D. when the chimeric mice was initially established for the HIV-1 study is indicated with parenthesis
†The source of human organs for the transplantation

mice were called SCID-hu thy/liv mice.[5] The SCID-hu thy/liv mice could support *de novo* generation of human T-cells including $CD4^+$ T-cells for more than one year and were highly susceptible to infection with HIV-1 (Table 1).[5–12] However, since the generation and the maintenance of human T-cells in the chimeric mice were mostly limited to the implanted organoid, direct inoculation of virus solution into the organoid is required. In addition, HIV-1 infection in SCID-hu thy/liv mice was restricted to the implanted organ, making the use of these models limited and exclusive for the studies on intrathymic infection with HIV-1 (Table 1). Moreover, due to the necessities of the surgical techniques and the ethical issues involved in other countries, such as Japan, HIV-1 studies using such thy/liv co-implanted SCID mice were mainly carried out in the USA.

In 1988, Mosier *et al.*[13] established a novel system, the hu-PBL-SCID mouse model. In 1991, the hu-PBL-SCID mice were initially utilized for an HIV-1 study (Table 1).[14] The hu-PBL-SCID mice are transplanted with human peripheral blood mononuclear cells (PBMCs) into the peritoneal cavity of several SCID mice, such as CB17-*scid* mice,[14–18] NOD-*scid* mice[19,20] and NOG mice.[21] Although transplanted human PBMCs including human $CD4^+$ T-cells circulated through the blood stream of recipient mice, because of graft-versus host disease (GVHD), the transplanted human PBMCs were highly activated and could only be maintained for a few months (Table 1).[22]

Humanized mouse models for HIV-1 infection

The variety of established humanized mouse models for HIV-1 studies

In 2004, Manz and colleagues[23] initially succeeded in establishing 'humanized mice' by transplanting human $CD34^+$ hematopoietic stem cells (hHSCs) into BALB/c-$Rag2^{-/-}\gamma_c^{-/-}$ mice. Humanized mice are mice that are transplanted with hHSCs and are therefore able to generate lineages of human leukocytes including $CD4^+$ T-cells *de novo*.

From 2006, lines of humanized mouse models for HIV-1 infection have been reported (Table 1).[24] As summarized in Table 2, the hHSC-transplanted humanized mice are mostly based on NOD.Cg-*Prkdc*^{scid} *Il2rg*^{tm1Sug}/Jic (NOG) mice,[25–28] NOD.Cg-*Prkdc*^{scid} *Il2rg*^{tm1Wjl}/SzJ (NSG) mice,[29,30] BALB/c-$Rag2^{-/-}\gamma_c^{-/-}$ mice[24,31–33] and H-2^d $Rag2^{-/-}\gamma_c^{-/-}$ mice.[34] NOG mice were established in the Central Institute for Experimental Animals (Kawasaki, Kanagawa, Japan), and it was reported that NOG mice lacked intrinsic murine T-cells and B-cells, and functional natural killer cells.[35] On the other hand, NSG mice were established in the Jackson Laboratory (Bar Harbor, ME, USA). Although both mice are sometimes synonymously called NOD/SCID/*Il2rg*$^{-/-}$ mice, the former has a defect in the transmembrane region of *Il2rg* gene (i.e. deletion of exon 7 of the gene), while the latter has a defect on the entire *Il2rg* gene. Of note, one report clearly showed that human $CD4^+$ T-cells in human PBMC-transplanted SCID mice were abnormally activated, due to GVHD.[21] In contrast, hHSC-transplanted humanized mouse models have the potential to maintain a relatively natural physiological condition for a long period of time (e.g. more than one year[25]). Therefore, the difference in the activation state of human T-cells in the murine system is of particular importance for understanding the significance of hHSC-transplanted humanized mice in comparison to human PBMC-transplanted mice.

In addition to the variety of recipient mice, the ways to construct humanized mice are also various: the age for hHSC transplantation (neonate or adult), the route for the transplantation (e.g. intrahepatic, intravenous or intraperitoneal injection) and the source of hHSCs (e.g. cord blood or fetal liver) (Table 2). Although it is still uncertain whether the construction method for humanized mice affects the efficiency of human hematopoiesis and the functionality of reconstituted human leukocytes, it has been suggested that the human immune system is more efficiently reconstituted in newborn recipients transplanted with hHSCs than that in adult recipients.[23]

As one of the 'up-graded' humanized mouse models, BLT (bone marrow/liver/thymus) mice has been recently established.[36] BLT mice are mice that are surgically implanted with organoids consisting of human fetal thymus and liver and are further transplanted with hHSCs. Although BLT mice are likely to possess the potential to reconstitute human hematopoiesis more effectively than the other 'conventional' hHSC-transplanted humanized mice, how to construct the BLT mouse model includes ethical problems because of the need for organs donated from aborted human fetuses.

Advantages of humanized mice for HIV-1 studies

So, what was the breakthrough in humanized mice for HIV-1 studies? When we set out to investigate HIV-1 infection and

Table 2 Establishment of HIV-1-infected humanized mice model and basic investigations

Reference	Designation*	Recipient mouse			Source of hHSCs**	HIV-1 strain††	Brief observations			PMID†††
		Strain†	Age‡	Route§			Virological‡‡	Pathological§§	Immunological***	
24	-	BALB/c-Rag2$^{-/-}\gamma c^{-/-}$	Neonate	i.h.	CB	YU-2 (R5), NL4-3 (X4)	**A, C**	**F**	**L (partial)**	17038503
25	NOG-hCD34 mice	NOG	Neonate	i.h.	CB	JR-CSF (R5), NL4-3 (X4)	**A, C**	**F, G**	**n/a**	19744686
26	NOG-hCD34 mice	NOG	Neonate	i.h.	CB	JR-CSF (R5)	**A, C**	**F**	**J, L (partial)**	20510741
27	hNOG mice	NOG	6–10 weeks old	i.v.	CB	JR-CSF (R5), MNp (X4)	**A, B**	**F**	**L**	16954502
28	hNOG mice‡‡‡	NOG	6–10 weeks old	i.v.	CB	JR-CSF (R5), MNp (X4), NL4-3 (X4)	**A, B, C**	**F, G**	**n/a**	17881441
29	BLT mice	NSG		Refer to the footnote§§§		LAI (X4)	**A, C, D**	**F, G, I**	**J, L**	17389241
30	BLT mice	NSG		Refer to the footnote§§§		ADA (R5), JR-CSF (R5)	**A, C**	**F**	**J, K, L**	19420076
31	DKO-hu HSC mice	BALB/c-Rag2$^{-/-}\gamma c^{-/-}$	Neonate	i.h.	CB or FL	JR-CSF (R5), NL4-3 (X4), NL-R3A (R5X4)	**A, C, E**	**F**	**n/a**	17132723
32	RAG-hu mice	BALB/c-Rag2$^{-/-}\gamma c^{-/-}$	Neonate	i.h.	FL	BaL (R5), NL4-3 (X4)	**A, B, C, E**	**F, G**	**n/a**	17078891
33	HIS mice	BALB/c-Rag2$^{-/-}\gamma c^{-/-}$	Neonate	i.h.	CB	ADA (R5), C1157 (R5)	**C, D**	**F, H**	**n/a**	17182671
34	HIS-Rag2$^{-/-}\gamma c^{-/-}$ mice	H-2^{d} Rag2$^{-/-}\gamma c^{-/-}$	Neonate	i.p.	FL	NFN-SX SL9 (R5)	**E**	**F**	**L (no)**	17314230

CB, cord blood; FL, fetal liver; n/a, not applicable

*The designation of the constructed humanized mice model named by the authors

†The strain of recipient mouse. NOG, NOD.Cg-*Prkdc*^{scid}*Il2rg*^{tm1Sug}/Jic (established in Central Institute for Experimental Animals, Kawasaki, Kanagawa, Japan); NSG, NOD.Cg-*Prkdc*^{scid}*Il2rg*^{tm1Wjl}/SzJ) (established in the Jackson Laboratory, Bar Harbor, Maine, USA)

‡The age of recipient mice for the transplantation

§The route for the transplantation. i.h., intrahepatic; i.v., intravenous; i.p., intraperitoneal

**The source of human CD34^{+} hematopoietic stem cells (hHSCs)

††The HIV-1 strains used in each study. The co-receptor usage of each HIV-1 strain was indicated with parenthesis. R5, CCR5-tropic; X4, CXCR4-tropic; R5X4, CCR5/CXCR4 dual-tropic

‡‡Virological observations: **A**, HIV-1 RNA in plasma; **B**, HIV-1 DNA in tissue(s); **C**, HIV-1-infected cells; **D**, HIV-1 antigen(s) in plasma; **E**, HIV-1 replication by *ex vivo* co-culture with the cells susceptible for HIV-1

§§Pathological observations: **F**, loss of CD4^{+} T-cells in peripheral blood (PB) or decrease of CD4/CD8 ratio in PB; **G**, thymopathy; **H**, lymphadenopathy; **I**, HIV-1 infection and depletion of CD4^{+} T-cells in gut-associated lymphoid tissues

***Immunological observations: **J**, expansion/activation of CD8^{+} T-cells in PB; **K**, detection of HLA-restricted HIV-1 antigen-specific CD8^{+} T-cells; **L**, analysis on anti-HIV-1 antigen antibodies in plasma/serum. Note that the extent of the detected antibodies was indicated with parenthesis

†††The PMID of each paper in PubMed (http://www.ncbi.nlm.nih.gov/pubmed/)

‡‡‡This hNOG mice were constructed without irradiation before the transplantation of hHSCs

§§§Fetal liver and thymus were surgically implanted under the kidney capsule of recipient mouse at 6–8 weeks old. After three weeks postimplantation, autologous FL-derived hHSCs were transplantd by i.v. injection

replication in primary $CD4^+$ T-cells *in vitro*, we usually have to activate the primary cells by using mitogens (e.g. anti-CD3 antibody, phytohemagglutinin and ionomycin) to support HIV-1 replication. On the other hand, as described above, hHSC-transplanted humanized mice are able to persistently maintain human hematopoiesis at a physiological condition. In addition, humanized mice possess a series of human $CD4^+$ T-cell subsets, including $CD45RA^+/CD45RO^-$ naïve, $CD45RA^-/CD45RO^+$ memory and $FOXP3^+$ regulatory cells. Moreover, humanized mice can support longitudinal HIV-1 expansion *in vivo* (see below). Taken together, humanized mice have several advantages for HIV-1 studies. When investigating the dynamics of HIV-1 infection, humanized mice have the potential to provide novel insights.

Basic observations in HIV-1-infected humanized mice

By using the constructed humanized mouse models, HIV-1 infection has been widely investigated based on virological, pathological and immunological issues (Table 2). For the investigation of HIV-1 infection *in vivo*, various HIV-1 strains including laboratory molecular clones and/or clinical isolates have been used. The phenotypes of HIV-1 can be distinguished by their co-receptor usage: CCR5 and/or CXCR4. From the clinical point of view, CCR5-tropic (R5) HIV-1 is broadly detected in patients. Prior to and/or during the rapid progression to AIDS in HIV-1-infected individuals, CCR5/CXCR4 dual-tropic (R5X4) HIV-1 can occasionally emerge, and then CXCR4-tropic (X4) HIV-1 can sometimes become predominant.[37] Therefore, in order to recapitulate HIV-1 pathogenesis in patients, it would be of importance to use R5 HIV-1 strains, such as JR-CSF and BaL, rather than X4 HIV-1.

Most HIV-1-infected humanized mice show persistent and longitudinal viremia in the plasma (Table 2), with the longest viremia reported for 30 weeks.[25] Also, virological evidence for HIV-1 infection, such as the detection of proviral DNA and infected cells, and HIV-1 replication by *ex vivo* co-culturing of cells isolated from the infected humanized mice with the cells susceptible for HIV-1 have been reported in previous literature (Table 2). Furthermore, one report revealed that the majority of HIV-1-producing cells (i.e. the cells positive for HIV-1 p24 antigen) in the spleen of infected humanized mice exhibited $CD45RA^-CD45RO^+CCR7^-$ effector memory phenotype and either or both $Ki67^+$ and/or $CD69^+$ activated/proliferating phenotype.[25] The paper also demonstrated the down-regulation of CD4 molecules on the surface of infected cells,[25] which would be caused by HIV-1-encoding proteins, such as Nef (negative factor), Vpu (viral protein U) and Env (envelope glycoprotein), as elucidated in-depth in *in vitro* studies.[38,39] Nevertheless, an extraordinary manner of viremia in HIV-1-humanized mice should be noted. In patients and SIV-infected macaques, viral load is initially fulminated at the acute phase. Then, the level of viral load declines through antiviral immune responses and is stably maintained at a set-point during the chronic phase. However, in HIV-1-infected humanized mice, a high level of viremia is longitudinally maintained without a reduction to the set-point.[24-32] Although the cause of the extraordinary manner of viremia in humanized mice is still uncertain, it is assumed that anti-HIV-1 adaptive immune responses are not sufficiently reconstituted in most humanized mice models (see below in detail).

Several pathological disorders, which are observed in HIV-1-infected patients, have been reproduced in HIV-1-infected humanized mice models (Table 2). For instance, the loss of $CD4^+$ T-cells (or the decline of the ratio of $CD4^+$ T-cells to $CD8^+$ T-cells) in peripheral blood (PB) of infected mice, which is one of the major pathological observations in patients, has been widely analyzed and demonstrated (Table 2). In addition, some papers showed thymopathy, which is mainly due to the depletion of $CD4^+$ thymocytes by HIV-1 infection. Moreover, an HIV-1-infected BLT mouse model demonstrated the infection and the depletion of $CD4^+$ T-cells residing in gut-associated lymphoid tissues, which has been proposed as one of the crucial steps in patients and SIV-infected rhesus macaque during the acute phase.[29]

Immune reaction against HIV-1 in infected mice has also been evaluated (Table 2). Although some papers showed the expansion and/or activation of $CD8^+$ T-cells in PB and tissues, it is yet unclear whether the expansion is triggered by HIV-1-specific human leukocyte antigen (HLA)-restricted reaction (see below in detail). Some papers also focused on humoral immunity against HIV-1; however, most HIV-1-infected humanized mice do not seem to induce the production of anti-HIV-1 antibodies (Table 2). Moreover, only one study demonstrated the HLA-restricted HIV-1 antigen-specific cellular immune response in HIV-1-infected BLT mice.[30]

Applications of HIV-1-infected humanized mice

In following the basic studies of HIV-1 infection in humanized mice (Table 2), some innovative investigations, which emphasized particular aspect(s) of HIV-1 infection *in vivo*, have been documented (Table 3). For instance, Ince *et al.*[40] analyzed the diversification and evolution of the R5 HIV-1 *env* gene in infected mice and detected the emergence of X4 HIV-1 *env* (Table 3a). Also, Jiang *et al.*[41] reported that $FOXP3^+$ regulatory T-cells were acutely and drastically depleted by HIV-1 infection in humanized mice, which suggests that $FOXP3^+$ regulatory T-cells are highly susceptible to HIV-1 *in vivo* (Table 3a). However, it is important to note that the virus used in the study was R5X4 HIV-1,[41] and that the observations reported need to be re-evaluated using R5 HIV-1. Moreover, a number of trials for the development of anti-HIV-1 therapies have been addressed (Table 3b) and will be described in-depth below.

Significance of host factors for HIV-1 infection *in vivo*

From an enormous amount of *in vitro* studies using cell culture systems, it has been well demonstrated that some cellular proteins have the potential to positively or negatively regulate HIV-1 replication and are called 'host factors'.[42] In respect to host factors positive for HIV-1 infection, CD4, CCR5 and/or CXCR4 on the surface of cells are utilized as the receptors for HIV-1 entry.[43,44] In addition, for the budding of nascent HIV-1 virions from the infected cell, HIV-1 hijacks cellular ESCRT (endosomal sorting

Table 3 Applications of HIV-1-infected humanized mice model

Reference	Designation*	Recipient mouse			Source of hHSCs**	HIV-1 strain††	Brief findings	PMID‡‡
		Strain†	Age‡	Route§				
(a) In-depth investigation of HIV-1 pathogenesis *in vivo*								
40	DKO-hu HSC mice	BALB/c-Rag2$^{-/-}\gamma c^{-/-}$	Neonate	i.h.	FL	NFN-SX SL9 (R5)	Mutation and evolution of HIV-1 *env* gene	20042504
41	DKO-hu HSC mice	BALB/c-Rag2$^{-/-}\gamma c^{-/-}$	Neonate	i.h.	FL	R3A (R5X4)	Acute infection and depletion of FOXP3$^+$ regulatory T-cells	18544681
64	NOG-hCD34 mice	NOG	Neonate	i.h.	CB	JR-CSF (R5), JR-CSFδ*vif* (R5)	Remarkable and lethal G-to-A mutation of HIV-1 DNA by APOBEC3 proteins	20610708
(b) Trials for anti-HIV-1 therapies								
65	hu-Rag2$^{-/-}\gamma c^{-/-}$ mice	BALB/c-Rag2$^{-/-}\gamma c^{-/-}$	Neonate	i.h.	FL	JR-CSF (R5)	Suppression of HIV-1 infection and recovery of peripheral CD4$^+$ T-cell loss by post-treatment with antiretroviral therapy	19494021
66	BLT mice	NSG		Refer to the footnote§§		JR-CSF (R5)	Prevention of vaginal HIV-1 transmission and systemic CD4$^+$ T-cell loss by PrEP***	18198941
67	BLT mice	NSG		Refer to the footnote§§		JR-CSF (R5)	Prevention of rectal and intravenous HIV-1 transmission by PrEP	20098623
72	hu-HSC mice	NSG	Neonate	i.v.	CB	BaL (R5)	Suppression of HIV-1 infection and recovery of peripheral CD4$^+$ T-cell loss by T cell-specific delivery of siRNAs against *CCR5*, and HIV-1 *tat* and *vif* genes using scFvCD7-9R†††	18691745
73	hu-BLT mice	NSG		Refer to the footnote‡‡‡		NFN-SX SL9 (R5), NL4-3 (X4)	Suppression of HIV-1 replication *ex vivo* by transduction of shRNA against *CCR5* using LV	20018916
74	-	NSG	Neonate	i.v.	CB	BaL (R5)	Supression of HIV-1 infection and recovery of peripheral CD4$^+$ T-cell loss by knock-out of *CCR5* gene using CCR5-targeted ZFN§§§	20601939

CB, cord blood; FL, fetal liver

*The designation of the constructed humanized mice model named by the authors

†The strain of recipient mouse. NOG, NOD.Cg-*Prkdc*^{scid} *Il2rg*^{tm1Sug}/Jic (established in Central Institute for Experimental Animals, Kawasaki, Kanagawa, Japan); NSG, NOD.Cg-*Prkdc*^{scid} *Il2rg*^{tm1Wjl}/SzJ (established in the Jackson Laboratory, Bar Harbor, Maine, USA)

‡The age of recipient mice for the transplantation

§The route for the transplantation. i.h., intrahepatic; i.v., intravenous; i.p., intraperitoneal

**The source of human CD34$^+$ hematopoietic stem cells (hHSCs)

††The HIV-1 strains used in each study. The co-receptor usage of each HIV-1 strain was indicated with parenthesis. R5, CCR5-tropic; X4, CXCR4-tropic; R5X4, CCR5/CXCR4 dual-tropic

‡‡The PMID of each paper in PubMed (http://www.ncbi.nlm.nih.gov/pubmed/)

§§Fetal liver and thymus were surgically implanted under the kidney capsule of recipient mouse at 6–8 weeks old. After three weeks postimplantation, autologous FL-derived hHSCs were transplanted by i.v. injection

***PrEP, pre-exposure prophylaxis

†††The CD7-specific single-chain antibody conjugated to oligo-9-arginine peptide (scFvCD7-9R), which was complexed to siRNAs, was administrated into the constructed hu-HSC mice by i.v. injection

‡‡‡FL hHSCs were transduced with lentivirus vector (LV) and solidified with Matrigel. Then the solidified LV-transduced FL hHSCs and fetal thymus were surgically implanted under the kidney capsule of recipient mouse at 6–8 weeks old. After 3 weeks postimplantation, the autologous LV-transduced FL hHSCs were transplantd by i.v. injection

§§§The plasmid expressing zinc-finger nuclease (ZFN) speficic for *CCR5* gene were nucleofected into hHSCs before transplantation

complex required for transport) machinery, which consists of TSG101 (tumor susceptibility gene 101),[45–47] CHMP (chromatin-modifying protein/charged multivesicular body protein) family proteins[48] and others.[49–53] On the other hand, APOBEC3 (apolipoprotein B mRNA-editing enzyme catalytic polypeptide-like 3) family proteins are one of the well-known host factors that can negatively regulate HIV-1 replication.[54,55]

APOBEC3s are cellular cytidine deaminases that convert cytosine in the viral minus-strand cDNA to uracil, resulting in the alteration of guanine (G) to adenine (A) in the nascent proviral DNA. Several APOBEC3 proteins are incorporated

into progeny virions and mutate viral cDNA in the invaded cells, which results in the inhibition of viral replication. On the other hand, an HIV-1 accessory protein, viral infectivity factor (Vif), has the ability to counteract the incorporation of certain APOBEC3 proteins such as APOBEC3G and APOBEC3F into progeny virions by degrading these proteins through the proteasome-dependent pathway.[56-59] Lines of *in vitro* investigations have elucidated the mechanisms of G-to-A hypermutation of HIV-1 DNA mediated by APOBEC3s and the counteracting ability of Vif against APOBEC3s, which have shed light on the relevance of host–retrovirus interaction.[60-63] Nevertheless, the physiological balance between intrinsic APOBEC3s and Vif *in vivo* has been poorly understood, and the significance of APOBEC3-mediated mutagenesis for HIV-1 replication *in vivo* has remained unresolved. In this regard, by using a humanized mice model, we have recently demonstrated the predominant accumulation of G-to-A mutations in *vif*-proficient (i.e. wild-type) HIV-1 provirus displaying characteristics of APOBEC3-mediated mutagenesis (Table 3a).[64] Notably, the APOBEC3-associated G-to-A mutation of HIV-1 DNA that leads to the termination of translation was significantly observed.[64] Furthermore, the paper provided a novel insight suggesting that HIV-1 G-to-A hypermutation is independently induced by individual APOBEC3 proteins. Taken together, these results provide evidence indicating that endogenous APOBEC3s are associated with G-to-A mutation of HIV-1 provirus *in vivo*, which can result in the abrogation of HIV-1 infection.

Trials for anti-HIV-1 therapies in humanized mice models

Since humanized mice are able to support persistent HIV-1 infection *in vivo*, humanized mice are also adequate for the evaluation of the efficiency of anti-HIV-1 strategies *in vivo*. In an effort to evaluate anti-HIV-1 trials *in vivo*, some attempts have been performed (Table 3b). Three papers have attempted to evaluate the effectiveness of anti-HIV-1 drugs, which have been already approved and are in clinical use, in HIV-1-infected humanized mice.[65-67] These reports strongly suggest that we will be able to evaluate the effectiveness of the candidates for novel anti-HIV-1 drugs in humanized mice as preclinical studies in the future.

It is well known that individuals who have a genetic defect in the *CCR5* gene, known as *CCR5Δ32*, are resistant to HIV-1 infection.[68-70] Interestingly, it has been recently reported that a bone marrow transplantation from a *CCR5Δ32* donor into a patient with HIV-1 infection and acute myeloid leukemia lead to the suppression of HIV-1 to levels below detection by conventional methods.[71] This result strongly suggests that the attenuation of *CCR5* gene expression (i.e. knock-down) and/or the disruption of the *CCR5* gene itself (i.e. knock-out) are effective and conceivable options for the suppression of HIV-1 expansion *in vivo*. In fact, as another strategy for the suppression of HIV-1 infection *in vivo*, genetic modifications of human hematopoietic cells in humanized mice models have been addressed. To knock-down/out the *CCR5* gene, several approaches have been reported. The first report showed that the administration of scFvCD7-9R (CD7-specific single-chain antibody conjugated to oligo-9-arginine peptide) complexed with siRNAs against *CCR5* and HIV-1-encoding genes efficiently delivered siRNAs into the T-cells of HIV-1-infected humanized mice and successfully suppressed R5 HIV-1 replication, leading to a recovery of $CD4^+$ T-cell loss in PB.[72] Second, the transduction of shRNA against *CCR5* using lentivirus vector into hHSCs prior to the transplantation into the recipient mice successfully attenuated *CCR5* expression in the $CD4^+$ T-cells differentiated in the constructed humanized mice.[73] The authors also showed that R5 HIV-1 replicated less efficiently in the $CD4^+$ T-cells isolated from the *CCR5*-targeted shRNA-transduced humanized mice *ex vivo*.[73] The third report used a zinc-finger nuclease (ZFN) technique that can target and digest specific nucleotide sequences in the cellular genome, which results in the knock-out of the targeted gene.[74] By nucleofection of *CCR5*-targeted ZFN-expressing plasmid into hHSCs before transplantation into the recipient mice, the researchers succeeded in the construction of *CCR5* knock-out humanized mice and showed suppression of HIV-1 infection and the recovery of $CD4^+$ T-cells in PB.[74] Taken together, these trials are crucial for the establishment of novel strategies to treat HIV-1 infection in patients. However, currently, it is still problematic that the efficiency of knock-down/out of *CCR5* gene in humanized mice is low. Therefore, it would be important to improve the technique(s) for knock-down/out of the target gene in the future. Moreover, as described above, there are several host factors that associate with HIV-1 replication other than CCR5. For instance, it has been already demonstrated that APOBEC3s endogenously expressed in $CD4^+$ T-cells can contribute to the diminution of HIV-1 expansion *in vivo*. Therefore, ectopic expression of APOBEC3s may be one of the effective strategies to abrogate HIV-1 infection *in vivo*.

Perspectives and remaining problems

Although humanized mice have several beneficial aspects for studies on HIV-1 infection and pathogenesis *in vivo*, it is also a fact that the humanized mice are still not perfect, particularly in terms of the reconstitution of acquired immunity. As summarized in Table 2, cellular and humoral immune responses observed in HIV-1-infected humanized mice are likely to be poorer than those in humans. It is thought that the inadequate acquired immune response, particularly cellular immunity, in humanized mice would be due to the thymic environment for the education of human T-cell precursors (i.e. thymocytes). In both humans and mice, it is well known that T-cell precursors are selected in the thymus by major histocompatibility complexes (MHCs) expressed on either or both thymic epithelial cells and/or dendritic cells. In humans, thymocytes are educated and are selected by HLAs (note that human MHC is also called HLA) expressed on thymic epithelial cells and/or dendritic cells. On the other hand, it is strongly suggested that human T-cell precursors in hHSC-transplanted humanized mice (with the exception of BLT mice) are selected and maturated in the murine thymic environment. However, it is still uncertain whether human thymocytes are selected by murine MHC molecules expressed on murine thymic cells or by other sources. In

this regard, it has been shown that mature T-cells can develop from cord blood-derived mononuclear cell cultures with supplementation of stem cell factors and interleukin-7 but without thymic feeder cells *in vitro*,[75] suggesting that the development of human T-cells in hHSC-transplanted humanized mice may be differentiated independent of murine MHCs. On the other hand, others have asserted that murine thymus can support human thymocyte differentiation via murine MHCs.[76,77]

To improve the functionality of human acquired immunity in hHSC-transplanted humanized mice, the genetic modification of the recipient mice has been performed. For example, two kinds of HLA-A2 transgenic (Tg) humanized mice have been independently established and reported. One was established by backcrossing NSG mice with HLA-A2.1 Tg mice,[78] while the other was constructed by backcrossing NSG mice with HLA-A2/HHD Tg mice.[79] Since these two humanized mice were able to mimic the human thymic microenvironment to some extent, human T-cells, especially $CD8^+$ T-cells, were successfully and more effectively educated by HLA-A2. In fact, it was reported that the differentiated $CD8^+$ T-cells in these HLA-A2 Tg humanized mice had the ability to elicit HLA-A2-restricted EBV-specific responses.[78,79] Therefore, these gains will lead to the improvement of humanized mouse models and is one of the most important directions to proceed in humanized mouse studies.

Concluding remarks

In conclusion, we herein documented the studies involving HIV-1 infection in humanized mouse models. To investigate the pathogenesis of AIDS, the SIV-infected rhesus macaque model has been widely used and accepted. However, conducting SIV/macaque experiments requires relatively high costs, and also it may be difficult to identify the findings in SIV/macaque models with those in patients with HIV-1 infection. On the other hand, conducting experiments using humanized mouse models demands relatively low cost, and can support and easily allow for monitoring of HIV-1 infection *in vivo*. Nevertheless, as described above, the dynamics of viral infection during the chronic phase in HIV-1-infected humanized mice are likely to be at variance with those in patients and SIV/macaque models. Namely, both the SIV-infected macaque models and the HIV-1-infected humanized mouse models have respective advantages and/or disadvantages. Therefore, to elucidate the *bona fide* HIV-1 pathogenesis *in vivo*, we believe that it would be important to mush-up the accumulated knowledge provided from SIV/macaque studies and novel findings from the studies on HIV-1-infected humanized mouse models.

Taken together, the humanized mice have the potential to investigate the dynamics of host–pathogen interaction *in vivo*. Using the humanized mouse models, we are able to combine strategies from multiple disciplines, which have been provided to us from the fields of molecular biology, clinical medicine and mathematical biology. This will in turn enable us to address unrevealed but essential aspects of human-specific pathogens including HIV-1.

Author contributions: KS and YK prepared the manuscript.

ACKNOWLEDGEMENTS

We would like to thank Peter Gee and Harmen Kloosterboer (Laboratory of Viral Pathogenesis, Institute for Virus Research, Kyoto University) for their assistance in proofreading this manuscript. This work was supported in-part by Grants-in-Aid for Scientific Research (B21390137, S22220007 to YK) from the Japan Society for the Promotion of Science; a Grant-in-Aid for Scientific Research on Priority Areas 'Matrix of Infection Phenomena' (18073008 to YK) from the Ministry of Education, Culture, Sports, Science and Technology of Japan; and Research on HIV/AIDS (200932025A to YK) from the Ministry of Health, Labor and Welfare of Japan.

REFERENCES

1 Anonymous. HIV vaccine failure prompts Merck to halt trial. *Nature* 2007;**449**:390
2 Shedlock DJ, Silvestri G, Weiner DB. Monkeying around with HIV vaccines: using rhesus macaques to define 'gatekeepers' for clinical trials. *Nat Rev Immunol* 2009;**9**:717–28
3 Watkins DI, Burton DR, Kallas EG, Moore JP, Koff WC. Nonhuman primate models and the failure of the Merck HIV-1 vaccine in humans. *Nat Med* 2008;**14**:617–21
4 Bosma GC, Custer RP, Bosma MJ. A severe combined immunodeficiency mutation in the mouse. *Nature* 1983;**301**:527–30
5 McCune JM, Namikawa R, Kaneshima H, Shultz LD, Lieberman M, Weissman IL. The SCID-hu mouse: murine model for the analysis of human hematolymphoid differentiation and function. *Science* 1988;**241**:1632–9
6 Namikawa R, Kaneshima H, Lieberman M, Weissman IL, McCune JM. Infection of the SCID-hu mouse by HIV-1. *Science* 1988;**242**:1684–6
7 McCune JM, Namikawa R, Shih CC, Rabin L, Kaneshima H. Suppression of HIV infection in AZT-treated SCID-hu mice. *Science* 1990;**247**:564–6
8 McCune J, Kaneshima H, Krowka J, Namikawa R, Outzen H, Peault B, Rabin L, Shih CC, Yee E, Lieberman M, Weissman I, Shultz L. The SCID-hu mouse: a small animal model for HIV infection and pathogenesis. *Annu Rev Immunol* 1991;**9**:399–429
9 Aldrovandi GM, Feuer G, Gao L, Jamieson B, Kristeva M, Chen IS, Zack JA. The SCID-hu mouse as a model for HIV-1 infection. *Nature* 1993;**363**:732–6
10 Bonyhadi ML, Rabin L, Salimi S, Brown DA, Kosek J, McCune JM, Kaneshima H. HIV induces thymus depletion *in vivo*. *Nature* 1993;**363**:728–32
11 Stanley SK, McCune JM, Kaneshima H, Justement JS, Sullivan M, Boone E, Baseler M, Adelsberger J, Bonyhadi M, Orenstein J, Fox CH, Fauci AS. Human immunodeficiency virus infection of the human thymus and disruption of the thymic microenvironment in the SCID-hu mouse. *J Exp Med* 1993;**178**:1151–63
12 Kaneshima H, Su L, Bonyhadi ML, Connor RI, Ho DD, McCune JM. Rapid-high, syncytium-inducing isolates of human immunodeficiency virus type 1 induce cytopathicity in the human thymus of the SCID-hu mouse. *J Virol* 1994;**68**:8188–92
13 Mosier DE, Gulizia RJ, Baird SM, Wilson DB. Transfer of a functional human immune system to mice with severe combined immunodeficiency. *Nature* 1988;**335**:256–9
14 Mosier DE, Gulizia RJ, Baird SM, Wilson DB, Spector DH, Spector SA. Human immunodeficiency virus infection of human-PBL-SCID mice. *Science* 1991;**251**:791–4
15 Mosier DE, Gulizia RJ, MacIsaac PD, Torbett BE, Levy JA. Rapid loss of $CD4^+$ T cells in human-PBL-SCID mice by noncytopathic HIV isolates. *Science* 1993;**260**:689–92
16 Gulizia RJ, Collman RG, Levy JA, Trono D, Mosier DE. Deletion of *nef* slows but does not prevent CD4-positive T-cell depletion in human immunodeficiency virus type 1-infected human-PBL-SCID mice. *J Virol* 1997;**71**:4161–4
17 Picchio GR, Gulizia RJ, Mosier DE. Chemokine receptor CCR5 genotype influences the kinetics of human immunodeficiency virus type 1 infection in human PBL-SCID mice. *J Virol* 1997;**71**:7124–7

18 Picchio GR, Gulizia RJ, Wehrly K, Chesebro B, Mosier DE. The cell tropism of human immunodeficiency virus type 1 determines the kinetics of plasma viremia in SCID mice reconstituted with human peripheral blood leukocytes. *J Virol* 1998;**72**:2002-9

19 Koyanagi Y, Tanaka Y, Kira J, Ito M, Hioki K, Misawa N, Kawano Y, Yamasaki K, Tanaka R, Suzuki Y, Ueyama Y, Terada E, Tanaka T, Miyasaka M, Kobayashi T, Kumazawa Y, Yamamoto N. Primary human immunodeficiency virus type 1 viremia and central nervous system invasion in a novel hu-PBL-immunodeficient mouse strain. *J Virol* 1997;**71**:2417-24

20 Miura Y, Misawa N, Maeda N, Inagaki Y, Tanaka Y, Ito M, Kayagaki N, Yamamoto N, Yagita H, Mizusawa H, Koyanagi Y. Critical contribution of tumor necrosis factor-related apoptosis-inducing ligand (TRAIL) to apoptosis of human $CD4^+$ T cells in HIV-1-infected hu-PBL-NOD-SCID mice. *J Exp Med* 2001;**193**:651-60

21 Nakata H, Maeda K, Miyakawa T, Shibayama S, Matsuo M, Takaoka Y, Ito M, Koyanagi Y, Mitsuya H. Potent anti-R5 human immunodeficiency virus type 1 effects of a CCR5 antagonist, AK602/ONO4128/GW873140, in a novel human peripheral blood mononuclear cell nonobese diabetic-SCID, interleukin-2 receptor gamma-chain-knocked-out AIDS mouse model. *J Virol* 2005;**79**:2087-96

22 Sandhu J, Shpitz B, Gallinger S, Hozumi N. Human primary immune response in SCID mice engrafted with human peripheral blood lymphocytes. *J Immunol* 1994;**152**:3806-13

23 Traggiai E, Chicha L, Mazzucchelli L, Bronz L, Piffaretti JC, Lanzavecchia A, Manz MG. Development of a human adaptive immune system in cord blood cell-transplanted mice. *Science* 2004;**304**: 104-7

24 Baenziger S, Tussiwand R, Schlaepfer E, Mazzucchelli L, Heikenwalder M, Kurrer MO, Behnke S, Frey J, Oxenius A, Joller H, Aguzzi A, Manz MG, Speck RF. Disseminated and sustained HIV infection in $CD34^+$ cord blood cell-transplanted $Rag2^{-/-}\gamma c^{-/-}$ mice. *Proc Natl Acad Sci USA* 2006;**103**:15951-6

25 Nie C, Sato K, Misawa N, Kitayama H, Fujino H, Hiramatsu H, Heike T, Nakahata T, Tanaka Y, Ito M, Koyanagi Y. Selective infection of $CD4^+$ effector memory T lymphocytes leads to preferential depletion of memory T lymphocytes in R5 HIV-1-infected humanized NOD/SCID/IL-$2Rg^{null}$ mice. *Virology* 2009;**394**:64-72

26 Sato K, Nie C, Misawa N, Tanaka Y, Ito M, Koyanagi Y. Dynamics of memory and naive $CD8^+$ T lymphocytes in humanized NOD/SCID/IL-$2Rg^{null}$ mice infected with CCR5-tropic HIV-1. *Vaccine* 2010;**28**(Suppl.2):B32-7

27 Watanabe S, Terashima K, Ohta S, Horibata S, Yajima M, Shiozawa Y, Dewan MZ, Yu Z, Ito M, Morio T, Shimizu N, Honda M, Yamamoto N. Hematopoietic stem cell-engrafted NOD/SCID/IL2Rg^{null} mice develop human lymphoid systems and induce long-lasting HIV-1 infection with specific humoral immune responses. *Blood* 2007;**109**: 212-8

28 Watanabe S, Ohta S, Yajima M, Terashima K, Ito M, Mugishima H, Fujiwara S, Shimizu K, Honda M, Shimizu N, Yamamoto N. Humanized NOD/SCID/IL2Rg^{null} mice transplanted with hematopoietic stem cells under nonmyeloablative conditions show prolonged life spans and allow detailed analysis of human immunodeficiency virus type 1 pathogenesis. *J Virol* 2007;**81**:13259-64

29 Sun Z, Denton PW, Estes JD, Othieno FA, Wei BL, Wege AK, Melkus MW, Padgett-Thomas A, Zupancic M, Haase AT, Garcia JV. Intrarectal transmission, systemic infection, and $CD4^+$ T cell depletion in humanized mice infected with HIV-1. *J Exp Med* 2007;**204**: 705-14

30 Brainard DM, Seung E, Frahm N, Cariappa A, Bailey CC, Hart WK, Shin HS, Brooks SF, Knight HL, Eichbaum Q, Yang YG, Sykes M, Walker BD, Freeman GJ, Pillai S, Westmoreland SV, Brander C, Luster AD, Tager AM. Induction of robust cellular and humoral virus-specific adaptive immune responses in human immunodeficiency virus-infected humanized BLT mice. *J Virol* 2009;**83**:7305-21

31 Zhang L, Kovalev GI, Su L. HIV-1 infection and pathogenesis in a novel humanized mouse model. *Blood* 2007;**109**:2978-81

32 Berges BK, Wheat WH, Palmer BE, Connick E, Akkina R. HIV-1 infection and CD4T cell depletion in the humanized $Rag2^{-/-}gc^{-/-}$ (RAG-hu) mouse model. *Retrovirology* 2006;**3**:76

33 Gorantla S, Sneller H, Walters L, Sharp JG, Pirruccello SJ, West JT, Wood C, Dewhurst S, Gendelman HE, Poluektova L. Human immunodeficiency virus type 1 pathobiology studied in humanized BALB/c-$Rag2^{-/-}\gamma c^{-/-}$ mice. *J Virol* 2007;**81**:2700-12

34 An DS, Poon B, Ho Tsong Fang R, Weijer K, Blom B, Spits H, Chen IS, Uittenbogaart CH. Use of a novel chimeric mouse model with a functionally active human immune system to study human immunodeficiency virus type 1 infection. *Clin Vaccine Immunol* 2007;**14**:391-6

35 Ito M, Hiramatsu H, Kobayashi K, Suzue K, Kawahata M, Hioki K, Ueyama Y, Koyanagi Y, Sugamura K, Tsuji K, Heike T, Nakahata T. NOD/SCID/γc^{null} mouse: an excellent recipient mouse model for engraftment of human cells. *Blood* 2002;**100**:3175-82

36 Melkus MW, Estes JD, Padgett-Thomas A, Gatlin J, Denton PW, Othieno FA, Wege AK, Haase AT, Garcia JV. Humanized mice mount specific adaptive and innate immune responses to EBV and TSST-1. *Nat Med* 2006;**12**:1316-22

37 Koot M, van 't Wout AB, Kootstra NA, de Goede RE, Tersmette M, Schuitemaker H. Relation between changes in cellular load, evolution of viral phenotype, and the clonal composition of virus populations in the course of human immunodeficiency virus type 1 infection. *J Infect Dis* 1996;**173**:349-54

38 Lindwasser OW, Chaudhuri R, Bonifacino JS. Mechanisms of CD4 downregulation by the Nef and Vpu proteins of primate immunodeficiency viruses. *Curr Mol Med* 2007;**7**:171-84

39 Wildum S, Schindler M, Munch J, Kirchhoff F. Contribution of Vpu, Env, and Nef to CD4 down-modulation and resistance of human immunodeficiency virus type 1-infected T cells to superinfection. *J Virol* 2006;**80**:8047-59

40 Ince WL, Zhang L, Jiang Q, Arrildt K, Su L, Swanstrom R. Evolution of the HIV-1 env gene in the $Rag2^{-/-}\gamma c^{-/-}$ humanized mouse model. *J Virol* 2010;**84**:2740-52

41 Jiang Q, Zhang L, Wang R, Jeffrey J, Washburn ML, Brouwer D, Barbour S, Kovalev GI, Unutmaz D, Su L. $FoxP3^+CD4^+$ regulatory T cells play an important role in acute HIV-1 infection in humanized $Rag2^{-/-}\gamma C^{-/-}$ mice *in vivo*. *Blood* 2008;**112**:2858-68

42 Freed EO. HIV-1 and the host cell: an intimate association. *Trends Microbiol* 2004;**12**:170-7

43 Berger EA, Murphy PM, Farber JM. Chemokine receptors as HIV-1 coreceptors: roles in viral entry, tropism, and disease. *Annu Rev Immunol* 1999;**17**:657-700

44 McClure MO, Sattentau QJ, Beverley PC, Hearn JP, Fitzgerald AK, Zuckerman AJ, Weiss RA. HIV infection of primate lymphocytes and conservation of the CD4 receptor. *Nature* 1987;**330**:487-9

45 Garrus JE, von Schwedler UK, Pornillos OW, Morham SG, Zavitz KH, Wang HE, Wettstein DA, Stray KM, Cote M, Rich RL, Myszka DG, Sundquist WI. Tsg101 and the vacuolar protein sorting pathway are essential for HIV-1 budding. *Cell* 2001;**107**:55-65

46 Martin-Serrano J, Zang T, Bieniasz PD. HIV-1 and Ebola virus encode small peptide motifs that recruit Tsg101 to sites of particle assembly to facilitate egress. *Nat Med* 2001;**7**:1313-9

47 VerPlank L, Bouamr F, LaGrassa TJ, Agresta B, Kikonyogo A, Leis J, Carter CA. Tsg101, a homologue of ubiquitin-conjugating (E2) enzymes, binds the L domain in HIV type 1 $Pr55^{Gag}$. *Proc Natl Acad Sci USA* 2001;**98**:7724-9

48 Strack B, Calistri A, Craig S, Popova E, Gottlinger HG. AIP1/ALIX is a binding partner for HIV-1 p6 and EIAV p9 functioning in virus budding. *Cell* 2003;**114**:689-99

49 Freed EO. The HIV-TSG101 interface: recent advances in a budding field. *Trends Microbiol* 2003;**11**:56-9

50 Fujii K, Hurley JH, Freed EO. Beyond Tsg101: the role of Alix in 'ESCRTing' HIV-1. *Nat Rev Microbiol* 2007;**5**:912-6

51 Carter CA. Tsg101: HIV-1's ticket to ride. *Trends Microbiol* 2002;**10**: 203-5

52 Morita E, Sandrin V, Alam SL, Eckert DM, Gygi SP, Sundquist WI. Identification of human MVB12 proteins as ESCRT-I subunits that function in HIV budding. *Cell Host Microbe* 2007;**2**:41-53

53 Kieffer C, Skalicky JJ, Morita E, De Domenico I, Ward DM, Kaplan J, Sundquist WI. Two distinct modes of ESCRT-III recognition are required for VPS4 functions in lysosomal protein targeting and HIV-1 budding. *Dev Cell* 2008;**15**:62-73

54 Sheehy AM, Gaddis NC, Choi JD, Malim MH. Isolation of a human gene that inhibits HIV-1 infection and is suppressed by the viral Vif protein. *Nature* 2002;**418**:646-50

55 Izumi T, Shirakawa K, Takaori-Kondo A. Cytidine deaminases as a weapon against retroviruses and a new target for antiviral therapy. *Mini Rev Med Chem* 2008;**8**:231–8

56 Marin M, Rose KM, Kozak SL, Kabat D. HIV-1 Vif protein binds the editing enzyme APOBEC3G and induces its degradation. *Nat Med* 2003;**9**:1398–403

57 Sheehy AM, Gaddis NC, Malim MH. The antiretroviral enzyme APOBEC3G is degraded by the proteasome in response to HIV-1 Vif. *Nat Med* 2003;**9**:1404–7

58 Shirakawa K, Takaori-Kondo A, Kobayashi M, Tomonaga M, Izumi T, Fukunaga K, Sasada A, Abudu A, Miyauchi Y, Akari H, Iwai K, Uchiyama T. Ubiquitination of APOBEC3 proteins by the Vif-Cullin5–ElonginB–ElonginC complex. *Virology* 2006;**344**:263–6

59 Stopak K, de Noronha C, Yonemoto W, Greene WC. HIV-1 Vif blocks the antiviral activity of APOBEC3G by impairing both its translation and intracellular stability. *Mol Cell* 2003;**12**:591–601

60 Chiu YL, Greene WC. The APOBEC3 cytidine deaminases: an innate defensive network opposing exogenous retroviruses and endogenous retroelements. *Annu Rev Immunol* 2008;**26**:317–53

61 Cullen BR. Role and mechanism of action of the APOBEC3 family of antiretroviral resistance factors. *J Virol* 2006;**80**:1067–76

62 Yu Q, Konig R, Pillai S, Chiles K, Kearney M, Palmer S, Richman D, Coffin JM, Landau NR. Single-strand specificity of APOBEC3G accounts for minus-strand deamination of the HIV genome. *Nat Struct Mol Biol* 2004;**11**:435–42

63 Yu X, Yu Y, Liu B, Luo K, Kong W, Mao P, Yu XF. Induction of APOBEC3G ubiquitination and degradation by an HIV-1 Vif-Cul5-SCF complex. *Science* 2003;**302**:1056–60

64 Sato K, Izumi T, Misawa N, Kobayashi T, Yamashita Y, Ohmichi M, Ito M, Takaori-Kondo A, Koyanagi Y. Remarkable lethal G-to-A mutations in *vif*-proficient HIV-1 provirus by individual APOBEC3 proteins in humanized mice. *J Virol* 2010;**84**:9546–56

65 Choudhary SK, Rezk NL, Ince WL, Cheema M, Zhang L, Su L, Swanstrom R, Kashuba AD, Margolis DM. Suppression of human immunodeficiency virus type 1 (HIV-1) viremia with reverse transcriptase and integrase inhibitors, $CD4^+$ T-cell recovery, and viral rebound upon interruption of therapy in a new model for HIV treatment in the humanized $Rag2^{-/-}g_c^{-/-}$ mouse. *J Virol* 2009;**83**:8254–8

66 Denton PW, Estes JD, Sun Z, Othieno FA, Wei BL, Wege AK, Powell DA, Payne D, Haase AT, Garcia JV. Antiretroviral pre-exposure prophylaxis prevents vaginal transmission of HIV-1 in humanized BLT mice. *PLoS Med* 2008;**5**:e16

67 Denton PW, Krisko JF, Powell DA, Mathias M, Kwak YT, Martinez-Torres F, Zou W, Payne DA, Estes JD, Garcia JV. Systemic administration of antiretrovirals prior to exposure prevents rectal and intravenous HIV-1 transmission in humanized BLT mice. *PLoS One* 2010;**5**:e8829

68 Samson M, Libert F, Doranz BJ, Rucker J, Liesnard C, Farber CM, Saragosti S, Lapoumeroulie C, Cognaux J, Forceille C, Muyldermans G, Verhofstede C, Burtonboy G, Georges M, Imai T, Rana S, Yi Y, Smyth RJ, Collman RG, Doms RW, Vassart G, Parmentier M. Resistance to HIV-1 infection in Caucasian individuals bearing mutant alleles of the CCR-5 chemokine receptor gene. *Nature* 1996;**382**:722–5

69 Michael NL, Chang G, Louie LG, Mascola JR, Dondero D, Birx DL, Sheppard HW. The role of viral phenotype and CCR-5 gene defects in HIV-1 transmission and disease progression. *Nat Med* 1997;**3**:338–40

70 Liu R, Paxton WA, Choe S, Ceradini D, Martin SR, Horuk R, MacDonald ME, Stuhlmann H, Koup RA, Landau NR. Homozygous defect in HIV-1 coreceptor accounts for resistance of some multiply-exposed individuals to HIV-1 infection. *Cell* 1996;**86**:367–77

71 Hutter G, Nowak D, Mossner M, Ganepola S, Mussig A, Allers K, Schneider T, Hofmann J, Kucherer C, Blau O, Blau IW, Hofmann WK, Thiel E. Long-term control of HIV by *CCR5* Delta32/Delta32 stem-cell transplantation. *N Engl J Med* 2009;**360**:692–8

72 Kumar P, Ban HS, Kim SS, Wu H, Pearson T, Greiner DL, Laouar A, Yao J, Haridas V, Habiro K, Yang YG, Jeong JH, Lee KY, Kim YH, Kim SW, Peipp M, Fey GH, Manjunath N, Shultz LD, Lee SK, Shankar P. T cell-specific siRNA delivery suppresses HIV-1 infection in humanized mice. *Cell* 2008;**134**:577–86

73 Shimizu S, Hong P, Arumugam B, Pokomo L, Boyer J, Koizumi N, Kittipongdaja P, Chen A, Bristol G, Galic Z, Zack JA, Yang O, Chen IS, Lee B, An DS. A highly efficient short hairpin RNA potently down-regulates CCR5 expression in systemic lymphoid organs in the hu-BLT mouse model. *Blood* 2010;**115**:1534–44

74 Holt N, Wang J, Kim K, Friedman G, Wang X, Taupin V, Crooks GM, Kohn DB, Gregory PD, Holmes MC, Cannon PM. Human hematopoietic stem/progenitor cells modified by zinc-finger nucleases targeted to CCR5 control HIV-1 *in vivo*. *Nat Biotechnol* 2010;**28**:839–47

75 Sanchez M, Alfani E, Visconti G, Passarelli AM, Migliaccio AR, Migliaccio G. Thymus-independent T-cell differentiation *in vitro*. *Br J Haematol* 1998;**103**:1198–205

76 Robin C, Bennaceur-Griscelli A, Louache F, Vainchenker W, Coulombel L. Identification of human T-lymphoid progenitor cells in $CD34^+CD38^{low}$ and $CD34^+CD38^+$ subsets of human cord blood and bone marrow cells using NOD-SCID fetal thymus organ cultures. *Br J Haematol* 1999;**104**:809–19

77 Weekx SF, Snoeck HW, Offner F, De Smedt M, Van Bockstaele DR, Nijs G, Lenjou M, Moulijn A, Rodrigus I, Berneman ZN, Plum J. Generation of T cells from adult human hematopoietic stem cells and progenitors in a fetal thymic organ culture system: stimulation by tumor necrosis factor-a. *Blood* 2000;**95**:2806–12

78 Strowig T, Gurer C, Ploss A, Liu YF, Arrey F, Sashihara J, Koo G, Rice CM, Young JW, Chadburn A, Cohen JI, Munz C. Priming of protective T cell responses against virus-induced tumors in mice with human immune system components. *J Exp Med* 2009;**206**:1423–34

79 Shultz LD, Saito Y, Najima Y, Tanaka S, Ochi T, Tomizawa M, Doi T, Sone A, Suzuki N, Fujiwara H, Yasukawa M, Ishikawa F. Generation of functional human T-cell subsets with HLA-restricted immune responses in HLA class I expressing NOD/SCID/IL2rg^{null} humanized mice. *Proc Natl Acad Sci USA* 2010;**107**:13022–7

An Evolutionary Analysis of *RAC2* Identifies Haplotypes Associated with Human Autoimmune Diseases

Manuela Sironi,†[1] Franca Rosa Guerini,†[2] Cristina Agliardi,[2] Mara Biasin,[3] Rachele Cagliani,[1] Matteo Fumagalli,[1] Domenico Caputo,[2] Andrea Cassinotti,[4] Sandro Ardizzone,[4] Milena Zanzottera,[2] Elisabetta Bolognesi,[2] Stefania Riva,[1] Yasuyoshi Kanari,[5] Masaaki Miyazawa,[5] and Mario Clerici,*[2,6]

[1]Bioinformatics Laboratory, Scientific Institute IRCCS E. Medea, Bosisio Parini (LC), Italy

[2]Don C. Gnocchi Foundation ONLUS, IRCCS, Milan, Italy

[3]Department of Clinical Science, LITA Vialba, University of Milan, Milan, Italy

[4]Department of Clinical Sciences, Chair of Gastroenterology, Luigi Sacco University Hospital, Milan, Italy

[5]Department of Immunology, Kinki University School of Medicine, Osaka-Sayama, Osaka, Japan

[6]Department of Biomedical Sciences and Technologies LITA Segrate, University of Milan, Milan, Italy

†These authors contributed equally to this work.

***Corresponding author:** E-mail: mario.clerici@unimi.it.

Associate editor: Willie Swanson

Abstract

The human *RAC2* gene encodes a small GTP-binding protein with a pivotal role in immune activation and in the induction of peripheral immune tolerance through restimulation-induced cell death (RICD). Different human pathogens target the protein product of *RAC2*, suggesting that the gene may be subject to natural selection, and that variants in *RAC2* may affect immunological phenotypes in humans. We scanned the genomic region encompassing the entire transcription unit for the presence of putative noncoding regulatory elements conserved across mammals. This information was used to select two *RAC2* gene regions and analyze their intraspecific genetic diversity. Results suggest that a region covering the 3′ untranslated region has been a target of multiallelic balancing selection (or diversifying selection), and three major *RAC2* haplogroups occur in human populations. Haplotypes belonging to one of these clades are associated with increased susceptibility to multiple sclerosis ($P = 0.022$) and earlier onset of disease symptoms ($P = 0.025$). This same haplogroup is significantly more common in patients with Crohn's disease compared with healthy controls ($P = 0.048$). These data reinforce recent evidences that susceptibility alleles/haplotypes are shared among multiple autoimmune disorders and support a causal "role for *RAC2*" variants in the pathogenesis of autoimmune diseases. Other genes with a role in RICD have previously been associated with autoimmunity in humans, suggesting that this pathway and RAC2 may represent novel therapeutic targets in autoimmune disorders.

Key words: *RAC2*, balancing selection, haplotype, multiple sclerosis, Crohn's disease.

Introduction

The human *RAC2* (ras-related C3 botulinum toxin substrate 2) gene encodes a member of the Ras superfamily of GTP-binding proteins primarily expressed in cells of hematopoietic origin (reviewed in Heasman and Ridley 2008). The protein product of *RAC2* regulates several processes central to immune and inflammatory responses including proliferation of primary T cells and differentiation towards the Th1 subtype, dendritic cell migration, neutrophil nicotinamide adenine dinucleotide phosphatase oxidase activity, and B cell maturation (Knaus et al. 1991; Li et al. 2000, 2002; Kim and Dinauer 2001; Yu et al. 2001; Croker et al. 2002; Benvenuti et al. 2004; Decoursey and Ligeti 2005). Therefore, *RAC2* can be regarded as a pivotal gene in the elicitation of immune responses, but it also plays a role in the induction of peripheral immune tolerance. Indeed, RAC2 represents an essential component of restimulation-induced cell death (RICD) via the Fas/FasL pathway (Ramaswamy et al. 2007).

Genes involved in immune response are believed to be frequent targets of natural selection (reviewed in Hurst 2009; Barreiro and Quintana-Murci 2010); in particular, balancing selection, which is thought to be a relatively rare phenomenon in humans (Asthana et al. 2005; Charlesworth 2006), has targeted a few genes involved in both innate and adaptive immunity (Ferrer-Admetlla et al. 2008; Barreiro and Quintana-Murci 2010; Sironi and Clerici 2010). This observation has been explained by the need to finely tune effective responses to pathogens on one side and development of pathogenic autoimmune/inflammatory reactions on the other (Ferrer-Admetlla et al. 2008). Yet, the role of autoimmunity and chronic inflammatory diseases as selective pressure during the course of human evolutionary history remains to be evaluated. Therefore, the maintenance of susceptibility alleles for autoimmune diseases may also be regarded as a possible by-product of adaptation to pathogen exposure (reviewed

in Sironi and Clerici 2010). In line with this view, susceptibility alleles for several human diseases have been shown to have increased in frequency in human populations as a result of recent positive selection (Barreiro and Quintana-Murci 2010), and several alleles that predispose to inflammatory bowel disease (IBD) have been a target of pathogen-driven selection (Fumagalli, Pozzali, et al. 2009). These observations suggest that past selective pressures exerted by infectious agents might have contributed to shaping the frequency spectrum of susceptibility alleles for autoimmune diseases.

Irrespective of the underlying mechanisms responsible for the maintenance of genetic diversity in humans, the identification of genes/gene regions subjected to natural selection can provide relevant information for the identification of functional variants that may influence complex phenotypic traits.

Here, we integrated the analysis of inter- and intraspecies genetic diversity to analyze the evolutionary pattern of *RAC2* and demonstrate its role as a susceptibility gene for multiple sclerosis (MS) and Crohn's disease (CD).

Materials and Methods

Analysis of Functional Elements and Sequence Conservation

Data concerning DNaseI hypersensitive sites in CD4+ T cells derive from a previous work (Boyle et al. 2008) and were retrieved from the University of California–San Cruz (UCSC) annotation tables (http://genome.ucsc.edu, Duke DNaseI HS track). PhastCons elements were derived from the UCSC website (tracks: phastConsElements44wayPlacMamm and phastConsElements44wayPrimates). Only conserved elements longer than 15 bp were considered. Similarly, information on histone marks was obtained from UCSC annotation tracks (ENCODE Integrated Regulation Tracks).

HapMap Samples and Sequencing

Human genomic DNA for the three human HapMap populations (Europeans, CEU; Yoruba, YRI; and Asian, AS) was obtained from the Coriell Institute for Medical Research. The two regions in *RAC2* were polymerase chain reaction (PCR) amplified and directly sequenced; primer sequences are available upon request. PCR products were treated with ExoSAP-IT (USB Corporation, Cleveland, OH), directly sequenced on both strands with a Big Dye Terminator sequencing Kit (v3.1, Applied Biosystems, Foster City, CA) and run on an Applied Biosystems ABI 3130 XL Genetic Analyzer (Applied Biosystems). Sequences were assembled using AutoAssembler version 1.4.0 (Applied Biosystems) and inspected manually by two distinct operators.

Patients, Controls, and Genotyping

For the MS case/control association study, a total of 722 individuals were enrolled: 387 relapsing-remitting multiple sclerosis (RRMS) patients (266 females and 121 males) and 335 age- and sex-matched healthy individuals (206 females and 129 males) of the same geographic origin (collection site). All patients and controls were Italians of Caucasian ethnicity. The RRMS patients were followed by MS Center of Don Gnocchi Foundation in Milan, Italy. Median age was 41.9 $\pm$ 10.9 and 42.32 $\pm$ 22.05 years for RRMS and controls, respectively. All patients underwent a standard battery of examinations, including medical history, physical and neurological examination, screening laboratory test, and brain magnetic resonance imaging. All patients with MS fulfilled the McDonald's criteria (McDonald et al. 2001). As for the CD case/control study, we recruited 313 individuals: 149 suffering from CD (96 males and 53 females) and 164 age- and sex-matched healthy individuals (104 males and 60 females). All subjects were Italians of Caucasian ethnicity. Patients referred since diagnosis to the IBD Unit of the Luigi Sacco Hospital in Milano, a third level center for the management of IBD patients, were enrolled. The diagnosis of CD was based on international published criteria, according to clinical, endoscopic, histological, and/or radiological data (Lennard-Jones 1989). A detailed clinical history, as well as laboratory and instrumental diagnostic data, were collected.

This study was designed and carried out in accordance with the Helsinki Declaration. Only patients signing an informed consent form were enrolled in the study, which was approved by the institutional review board.

All RRMS subjects were genotyped for the *HLA-DRB1* locus by sequence-specific primed PCR using Histo Type DNA well plates (BAG, Formedic diagnostici, Milan, Italy).

Genomic DNA was used as template for PCR amplification using TaqMan probes specifically designed to perform a single nucleotide polymorphism (SNP) genotyping assay for rs2899284 (A/G) and rs739041 (A/G) (TaqMan SNP genotyping assay; Applied Biosystems) and using the allelic discrimination real-time PCR method. The PCR consisted of a hot start at 95 °C for 10 min followed by 40 cycles of 94 °C for 15 s and 60 °C for 1 min. Fluorescence detection took place at a temperature of 60 °C. All assays were performed in 10 μl reactions, using TaqMan Genotyping Master Mix on 96-well plates using an ABI 7000 instrument (Applied Biosystems). After Bonferroni correction, the two SNPs complied to Hardy–Weinberg equilibrium (HWE) in all cohorts.

As for the 15 null SNPs used to test for population structure, TaqMan SNP genotyping assays were also used with the same conditions detailed above. The dbSNP IDs and reported minor allele frequencies in CEU were as follows: rs10113320 (0.319), rs10488619 (0.42), rs10785952 (0.363), rs12313915 (0.332), rs12618959 (0.283), rs2220858 (0.362), rs2625956 (0.164), rs2842063 (0.159), rs310644 (0.111), rs6687440 (0.347), rs289816 (0.111), rs4783432 (0.161), rs6001728 (0.221), rs16877243 (0.192), rs1885167 (0.204). All SNPs were in HWE in both RRMS and control subjects.

Population Genetic Analysis

Tajima's *D* (Tajima 1989) and Fu and Li's D^* and F^* (Fu and Li 1993) statistics, as well as diversity parameters θ_w (Watterson 1975) and π (Nei and Li 1979), were calculated using "libsequence" (Thornton 2003), a C++ class library

providing an object-oriented framework for the analysis of molecular population genetic data. Calibrated coalescent simulations were performed using the "cosi" package (Schaffner et al. 2005) and its best-fit parameters for YRI, CEU, and AS populations with 10,000 iterations. Additional coalescent simulations were computed with the ms software (Hudson 2002) specifying the number of chromosomes; the mutation parameter estimated from the data and the recombination rate with 10,000 iterations for each demographic model. The other parameters for each model were set as previously proposed (Marth et al. 2004; Voight et al. 2005). The maximum likelihood ratio Hudson–Kreitman–Aguadé (MLHKA) test was performed using the MLHKA software (Wright and Charlesworth 2004), as previously proposed (Fumagalli, Cagliani, et al. 2009). Briefly, 16 reference loci were randomly selected among National Institute of Environmental Health Sciences (NIEHS) loci shorter than 20 kb that have been resequenced in the three populations; the only criterion was that Tajima's *D* statistic did not suggest the action of natural selection (i.e., Tajima's *D* statistic is higher than the 5th and lower than the 95th percentiles in the distribution of NIEHS genes). The reference set was accounted for by the following genes: *VNN3* (MIM 606592), *PLA2G2D* (MIM 605630), *MB* (MIM 160000), *MAD2L2* (MIM 604094), *HRAS* (MIM 190020), *CYP17A1* (MIM 609300), *ATOX1* (MIM 602270), *BNIP3* (MIM 603293), *CDC20* (MIM 603618), *NGB* (MIM 605304), *TUBA1* (MIM 191110), *MT3* (MIM 139255), *NUDT1* (MIM 600312), *PRDX5* (MIM 606583), *RETN* (MIM 605565), and *JUND* (MIM 165162). In all analyses, the chimpanzee was used as the outgroup.

Data Retrieval, Haplotype Construction, and TMRCA Calculation

Genotype data for 238 resequenced human genes were derived from the NIEHS SNPs Program Web site. In particular, we selected genes that had been resequenced in populations of defined ethnicity including CEU, YUI, and AS (NIEHS panel 2).

For HapMap samples, haplotypes were inferred using PHASE version 2.1 (Stephens et al. 2001; Stephens and Scheet 2005), a program for reconstructing haplotypes from unrelated genotype data through a Bayesian statistical method. Haplotypes for individuals resequenced in this study are available as supplementary table S1, Supplementary Material online.

The median-joining network was constructed using NETWORK 4.5 (Bandelt et al. 1999). Estimate of the time to the most recent common ancestor (TMRCA) was obtained using a maximum likelihood coalescent method implemented in GENETREE (Griffiths and Tavare 1994, 1995). The mutation rate μ was obtained on the basis of the divergence between human and chimpanzee, and under the assumption both that the species separation occurred 6 Ma (Glazko and Nei 2003) and of a generation time of 25 years. Using this μ, a maximum likelihood estimate of θ (θ_{ML}) of 8 was obtained, resulting in an estimated effective population size (N_e) of 16,260, a value comparable to most figures reported in the literature (Tishkoff and Verrelli 2003). With these assumptions, the coalescence time, scaled in $2N_e$ units, was converted into years. For the coalescence process, 10^6 simulations were performed.

Estimates of allelic richness and private allelic richness for the three observed haplogroups were derived via Monte Carlo simulations by applying a rarefaction procedure to account for differences in sample size among clades (Kalinowski 2004). Specifically, we performed 1,000 simulations by randomly drawing g chromosomes (with $g = 20$) without replacement within each haplogroup and counting the number of polymorphic variants and private alleles within each clade. The average number of polymorphisms and private variants in the simulated samples represents our estimate of allelic richness and private allelic richness.

Association Analysis and Population Structure

Haplotype association analysis was performed using PLINK (Purcell et al. 2007) by logistic regression. Haplotype probabilities of individual subjects were incorporated as covariates in the regression models, which estimate the odds ratios associated with having a specific haplotype under an additive model. Sex was also used as a covariate. Wald tests were used to calculate *P* values.

In order to test for the presence of population stratification, 15 "null" SNPs (IDs are reported above) were selected. Specifically, 15 SNPs from a panel of ancestry informative markers (Enoch et al. 2006) were selected to be located on different chromosomes and for having a minor allele frequency in HapMap CEU > 0.10. Using these data, the inflation factor λ (Devlin et al. 2001) was calculated through the use of the Genomic Control (GC) function in the SNPassoc R package (Gonzalez et al. 2007). For estimation of the ancestry proportion for each RRMS and control subject, we used STRUCTURE 2.1 (Pritchard et al. 2000; Falush et al. 2003) based on the genotype information of the 15 null SNPs. Simulation parameters were set to 100,000 burn-ins followed by 100,000 runs. The most common criterion to detect the true number of populations (K) is based on computing an estimate of the posterior probability of the data for a given K, L(K). However, choosing K which maximizes the value of L(K) tends to overestimate the true number of populations, especially when a correction for the correlated population allele frequencies is adopted (Evanno et al. 2005). To overcome this issue, we computed a statistics based on the second rate of change of L(K) with respect to the value of K, as previously proposed (Evanno et al. 2005). The peak of this new function detects the most likely value of K, which, in our case, was estimated to be equal to 2. Individual admixture estimates obtained from STRUCTURE 2.1 were added as continuous covariates (with haplotypes and sex) in a second logistic regression analysis to correct for possible cryptic substructure. Only 1 of the 2 ($K = 2$) admixture proportions was included because the two proportions sum to 1, making them collinear.

For analysis of association between specific *RAC2* haplotypes and age at onset, linear regression analyses were

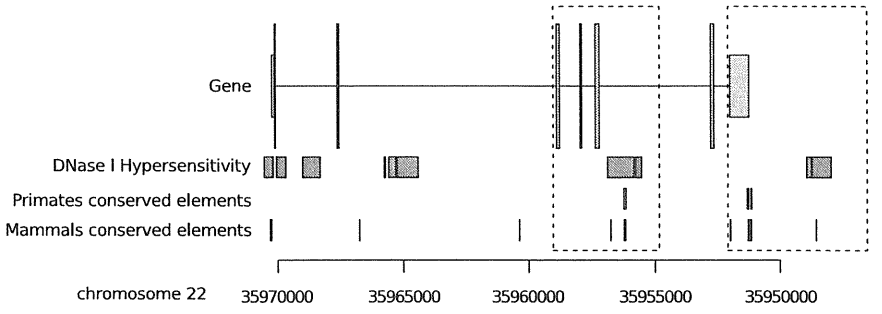

FIG. 1. Schematic diagram of the exon–intron structure of *RAC2*. Along the gene, gray boxes represent exons (coding regions and UTRs are denoted by having different height). The location of DNaseI hypersensitive sites in CD4+ T cells is shown below the gene diagram (green boxes). Noncoding conserved elements in primate (red) and placental mammals (blue) are also reported. The two regions selected for resequencing are delimited by the hatched lines.

performed using PLINK (Purcell et al. 2007). For RRMS subjects, presence/absence of the *HLA-DRB*15* allele was used a covariate in the regression.

Results

Analysis of Interspecies Sequence Conservation

Given the central role of RAC2 in immune responses, it is conceivable that variants located within or in proximity of the gene affect the susceptibility to infectious or autoimmune diseases in humans. If this were the case, such variants may also represent natural selection targets.

No nonsynonymous SNP in the gene has been described in dbSNP (Build 131, http://www.ncbi.nlm.nih.gov/projects/SNP); similarly, inspection of the 1000 Genomes Project data (http://browser.1000genomes.org) identified no amino acid replacement variant, suggesting that protein sequence variation in RAC2 does not contribute significantly to intraspecific and phenotypic diversity in human populations. Therefore, we aimed at identifying *RAC2* genic regions that may be more likely to harbor noncoding functional elements and, possibly, regulatory variants.

To this purpose, we relied on the concept whereby noncoding elements that are conserved across multiple species are more likely to be functional (Sironi et al. 2005). We scanned a genomic region covering the whole RAC2 transcription unit and flanking regions for the presence of DNaseI hypersensitive sites in CD4+ T cells, noncoding regions conserved in placental mammals, and noncoding sequences conserved across primates (see Materials and Methods for details). As reported in figure 1, two distinct regions displayed more than one conserved element and DNaseI hypersensitive sites: One is located in intron 5 and the other covers the 3′ untranslated region and a genomic portion downstream the transcription end site. We therefore selected these two regions, hereafter referred to as $RAC2_{in5}$ (4,202 bp) and $RAC2_{3'}$ (5,560 bp), for further analysis.

Nucleotide Diversity, Neutrality Tests, and Time Estimate

In order to get a complete view of the genetic diversity in $RAC2_{in5}$ and $RAC2_{3'}$, and analyze their evolutionary pattern in humans, we resequenced the two regions in three HapMap populations, namely YRI, CEU, and AS.

Overall, only one coding SNP was identified (Lys84Lys). For both regions, we calculated nucleotide diversity by means of two indexes: θ_w (Watterson 1975), an estimate of the expected per site heterozygosity, and π (Nei and Li 1979), the average number of pairwise sequence nucleotide differences. In order to compare the values we obtained for the two *RAC2* regions, we calculated θ_w and π for 5 kb regions deriving from 238 genes resequenced by the NIEHS program in the same population samples; the percentile rank corresponding to $RAC2_{in5}$ and $RAC2_{3'}$ in the distribution of values for NIEHS genes is reported in table 1 and indicates that $RAC2_{3'}$ displays extremely high nucleotide diversity in all populations; conversely, no exceptional values are observed for $RAC2_{in5}$. These data suggest that genetic diversity in the $RAC2_{3'}$ region might be maintained in human populations by a selective process (e.g., balancing selection).

Under neutral evolution, values of θ_w and π are expected to be roughly equal; for $RAC2_{3'}$, this is not verified, π being higher than θ_w in YRI and CEU (table 1). Tajima's *D* statistic (D_T) (Tajima 1989) was specifically developed to evaluate departure from neutrality by comparing θ_w and π; positive values of D_T indicate an excess of intermediate frequency variants and are a hallmark of balancing selection. Similarly to D_T, Fu and Li's F^* and D^* are based on SNP frequency spectra, but they also take into account whether mutations occur in external or internal branches of a genealogy (Fu and Li 1993). As population history, in addition to selective processes, is known to affect the site frequency spectrum (SFS) and all related statistics, we performed coalescent simulations using a population genetics model that incorporates demographic scenarios (Schaffner et al. 2005). As an empirical comparison, we also exploited the availability of 5 kb windows to obtain a reference distribution of SFS-based statistics in the three populations. Neutrality tests for $RAC2_{3'}$ suggested departure from neutrality in all populations with significantly positive values for at least one statistic in YRI and AS (table 1). In line with these results, the value of D_T in YRI and Fu and Li's D^* in AS were higher than the 95th percentile calculated over the distribution of NIEHS 5 kb windows. Conversely, no departure from